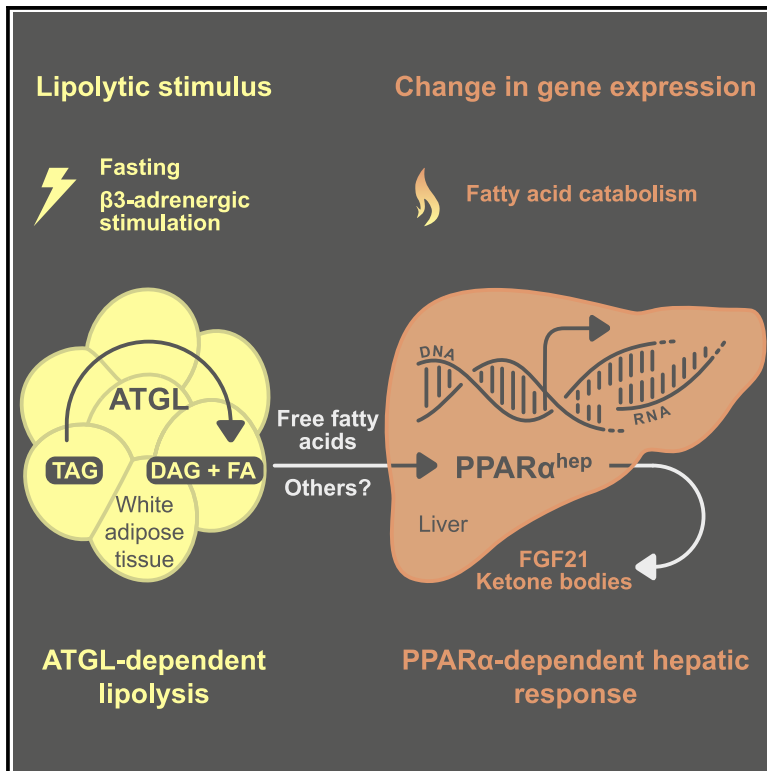


## ATGL-dependent white adipose tissue lipolysis controls hepatocyte PPAR $\alpha$ activity

### Graphical abstract



### Authors

Anne Fougerat, Gabriele Schoiswohl, Arnaud Polizzi, ..., Dominique Langin, Achim Lass, Hervé Guillou

### Correspondence

achim.lass@uni-graz.at (A.L.),  
herve.guillou@inrae.fr (H.G.)

### In brief

Fougerat et al. show that adipocyte ATGL is required for hepatic transcriptional responses during lipolysis induced by fasting and by stimulation of  $\beta_3$ -adrenergic receptor. Hepatocyte PPAR $\alpha$  is a key player of this adipose-to-liver cross-talk, regulating not only liver gene expression and homeostasis but also BAT activation.

### Highlights

- Adipocyte ATGL-dependent lipolysis controls liver gene expression in fasting
- Adipocyte ATGL regulates liver genes responsive to  $\beta_3$ -adrenergic stimulation
- The adipose to liver dialogue relies on gene expression control by hepatocyte PPAR $\alpha$
- Hepatocyte PPAR $\alpha$  influences BAT activation upon  $\beta_3$ -adrenergic stimulation



## Report

ATGL-dependent white adipose tissue lipolysis controls hepatocyte PPAR $\alpha$  activity

Anne Fougerat,<sup>1</sup> Gabriele Schoiswohl,<sup>2,3,4</sup> Arnaud Polizzi,<sup>1</sup> Marion Régnier,<sup>1</sup> Carina Wagner,<sup>2,3</sup> Sarra Smati,<sup>1,5</sup> Tiffany Fougerat,<sup>1</sup> Yannick Lippi,<sup>1</sup> Frederic Lasserre,<sup>1</sup> Ilyès Raho,<sup>6</sup> Valentine Melin,<sup>1</sup> Blandine Tramunt,<sup>7,8</sup> Raphaël Métivier,<sup>9</sup> Caroline Sommer,<sup>1</sup> Fadila Benhamed,<sup>10</sup> Chantal Alkhoury,<sup>11</sup> Franziska Greulich,<sup>12</sup> Céline Jouffe,<sup>13</sup> Anthony Emile,<sup>1</sup> Michael Schupp,<sup>14</sup> Pierre Gourdy,<sup>7,8</sup> Patricia Dubot,<sup>15,16</sup> Thierry Levade,<sup>15,16</sup> Delphine Meynard,<sup>17</sup> Sandrine Ellero-Simatos,<sup>1</sup> Laurence Gamet-Payastre,<sup>1</sup> Ganna Panasyuk,<sup>11</sup> Henriette Uhlenhaut,<sup>12,13</sup> Ez-Zoubir Amri,<sup>18</sup> Céline Cruciani-Guglielmacci,<sup>6</sup> Catherine Postic,<sup>10</sup> Walter Wahli,<sup>1,19,20</sup> Nicolas Loiseau,<sup>1</sup> Alexandra Montagner,<sup>7</sup> Dominique Langin,<sup>7,16,21</sup> Achim Lass,<sup>2,3,22,\*</sup> and Hervé Guillou<sup>1,22,23,\*</sup>

<sup>1</sup>Toxalim (Research Center in Food Toxicology), INRAE, ENVT, INP- PURPAN, UMR 1331, UPS, Université de Toulouse, Toulouse, France

<sup>2</sup>Institute of Molecular Biosciences, NAWI Graz, University of Graz, Heinrichstraße 31/II, 8010 Graz, Austria

<sup>3</sup>BioTechMed-Graz, Graz, Austria

<sup>4</sup>Department of Pharmacology and Toxicology, University of Graz, Humboldtstraße 46/II, 8010 Graz, Austria

<sup>5</sup>Nantes Université, CHU Nantes, CNRS, INSERM, l'Institut du Thorax, 44000 Nantes, France

<sup>6</sup>Université Paris Cité, BFA, UMR 8251, CNRS, 75013 Paris, France

<sup>7</sup>Institute of Metabolic and Cardiovascular Diseases, I2MC, University of Toulouse, INSERM, Toulouse III University - Paul Sabatier (UPS), Toulouse, France

<sup>8</sup>Service de Diabétologie, Maladies Métaboliques et Nutrition, CHU de Toulouse, Toulouse, France

<sup>9</sup>Institut de Génétique et Développement de Rennes, Université de Rennes, UMR 6290 CNRS, Rennes, France

<sup>10</sup>Institut Cochin, Université Paris Cité, CNRS, INSERM, F-75014 Paris, France

<sup>11</sup>Université Paris Cité, INSERM UMR-S1151, CNRS UMR-S8253, Institut Necker-Enfants Malades, F-75015 Paris, France

<sup>12</sup>Metabolic Programming, TUM School of Life Sciences, ZIEL Institute for Food & Health, Gregor-Mendel-Strasse 2, 85354 Freising, Germany

<sup>13</sup>Helmholtz Diabetes Center (IDO, IDC, IDE), Helmholtz Center Munich HMGU, Ingolstaedter Landstr. 1, 85764 Neuherberg, Germany

<sup>14</sup>Institute of Pharmacology, Charité-Universitätsmedizin Berlin, Corporate Member of Freie Universität Berlin, Humboldt-Universität zu Berlin, and Berlin Institute of Health, 10115 Berlin, Germany

<sup>15</sup>INSERM U1037, CRCT, Université Paul Sabatier, 31059 Toulouse, France

<sup>16</sup>Laboratoire de Biochimie, CHU Toulouse, Toulouse, France

<sup>17</sup>Institute of Digestive Health Research, IRSD, INSERM U1220, Toulouse, France

<sup>18</sup>Université Côte d'Azur, CNRS, INSERM, iBV, Nice, France

<sup>19</sup>Lee Kong Chian School of Medicine, Nanyang Technological University Singapore, Singapore 308232, Singapore

<sup>20</sup>Center for Integrative Genomics, University of Lausanne, Le Génopode, 1015 Lausanne, Switzerland

<sup>21</sup>Academic Institute of France (IUF), Paris, France

<sup>22</sup>These authors contributed equally

<sup>23</sup>Lead contact

\*Correspondence: [achim.lass@uni-graz.at](mailto:achim.lass@uni-graz.at) (A.L.), [herve.guillou@inrae.fr](mailto:herve.guillou@inrae.fr) (H.G.)

<https://doi.org/10.1016/j.celrep.2022.110910>

## SUMMARY

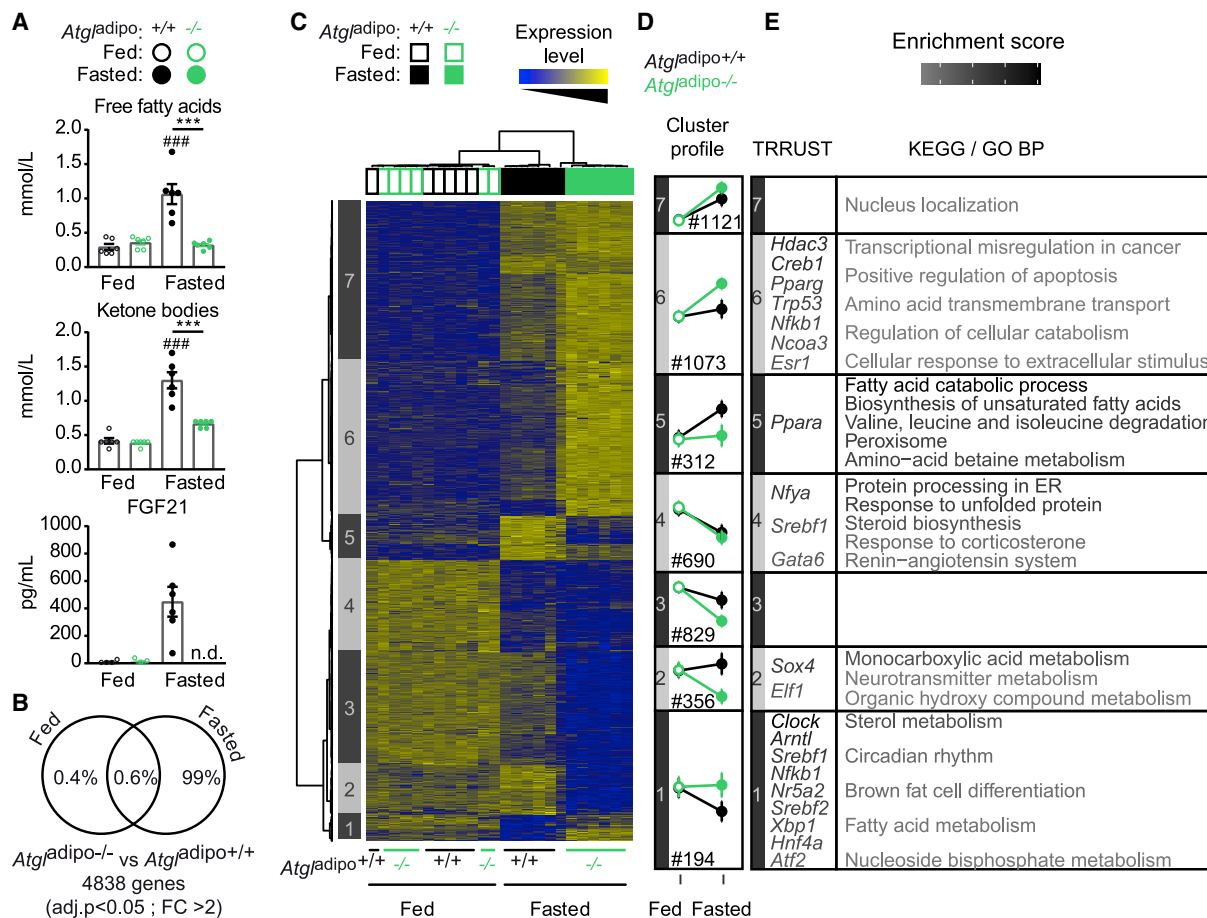
In hepatocytes, peroxisome proliferator-activated receptor  $\alpha$  (PPAR $\alpha$ ) orchestrates a genomic and metabolic response required for homeostasis during fasting. This includes the biosynthesis of ketone bodies and of fibroblast growth factor 21 (FGF21). Here we show that in the absence of adipose triglyceride lipase (ATGL) in adipocytes, ketone body and FGF21 production is impaired upon fasting. Liver gene expression analysis highlights a set of fasting-induced genes sensitive to both ATGL deletion in adipocytes and PPAR $\alpha$  deletion in hepatocytes. Adipose tissue lipolysis induced by activation of the  $\beta_3$ -adrenergic receptor also triggers such PPAR $\alpha$ -dependent responses not only in the liver but also in brown adipose tissue (BAT). Intact PPAR $\alpha$  activity in hepatocytes is required for the cross-talk between adipose tissues and the liver during fat mobilization.

## INTRODUCTION

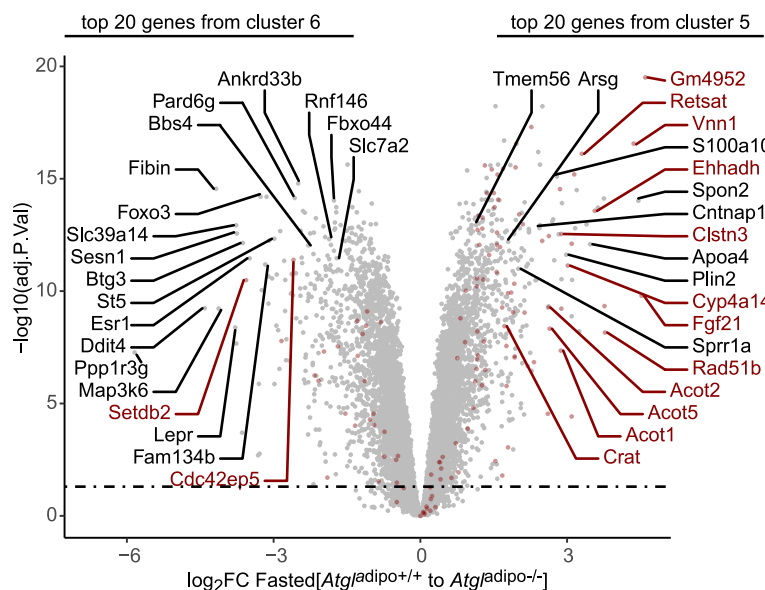
The liver plays a key role in the control of energy homeostasis in response to nutrient availability. Several transcription factors regulate hepatic genes involved in metabolic pathways to main-

tain energy homeostasis (Goldstein and Hager, 2015). Among these factors, peroxisome proliferator-activated receptor  $\alpha$  (PPAR $\alpha$ ) is critical for the adaptive response to fasting (Kersten et al., 1999; Montagner et al., 2016; Polizzi et al., 2016; Régnier et al., 2018). PPAR $\alpha$  is a ligand-activated transcription factor of

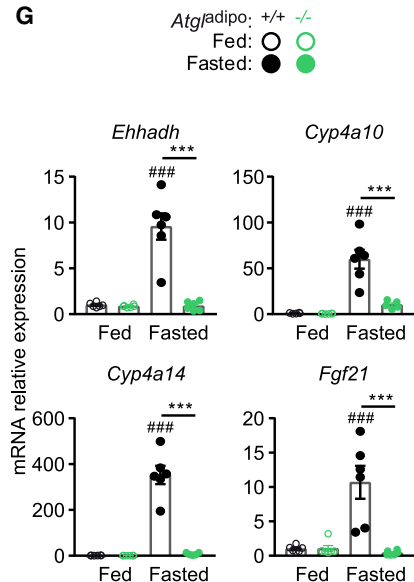




**F** • PPARα-driven expression during fasting



**G**



(legend on next page)

the nuclear receptor superfamily. Endogenous ligands of PPAR $\alpha$  include fatty acids and fatty-acid-derived lipids (Desvergne and Wahli, 1999). In hepatocytes, PPAR $\alpha$  controls the expression of genes involved in lipid catabolism during fasting (Kersten et al., 1999; Montagner et al., 2016; Régnier et al., 2018). Mice with hepatocyte-specific deletion of *Ppar $\alpha$*  have impaired ketone body production in response to fasting (Montagner et al., 2016). PPAR $\alpha$  is also required for the expression of fibroblast growth factor 21 (FGF21) (Badman et al., 2007; Inagaki et al., 2007; Iroz et al., 2017), a hepatokine with systemic metabolic effects (Han et al., 2021; Klierer and Mangelsdorf, 2019).

During fasting, white adipose tissue (WAT) lipolysis releases fatty acids that are delivered to the liver. Fatty acids are essential for fasting-induced expression of hepatic FGF21 (Jaeger et al., 2015). WAT lipolysis is required to fuel thermogenesis during fasting (Schreiber et al., 2017; Shin et al., 2017) and cold exposure (Chittraju et al., 2020; Heine et al., 2018).

It has been suggested that fatty acids released from WAT during fasting may act as PPAR $\alpha$  ligands (Jaeger et al., 2015). However, hepatic *de novo* fatty acid synthesis also provides ligands for PPAR $\alpha$ -regulated gene expression in the liver (Chakravarthy et al., 2005, 2009). Thus, the source of fatty acids that activate hepatic PPAR $\alpha$  during fasting remains to be clarified. Here, we identify adipose triglyceride lipase (ATGL)-dependent lipolysis as a regulator of hepatic function through the control of gene expression and hepatocyte PPAR $\alpha$  as a key player of this cross-talk between adipose tissues and the liver.

## RESULTS

### Adipocyte ATGL-dependent lipolysis is required for fasting-induced responses in the liver

To investigate the role of WAT lipolysis in hepatic homeostasis, we used *Atgl*<sup>adipo+/+</sup> and adipocyte-specific *Atgl* knockout mice (*Atgl*<sup>adipo-/-</sup>) (Schoiswohl et al., 2015), which were either fed *ad libitum* or fasted for 24 h. Adipocyte *Atgl* deletion reduced fasting-induced lipolysis as indicated by the absence of an increase in plasma free fatty acids (FFAs) in fasted *Atgl*<sup>adipo-/-</sup> mice (Figure 1A). Moreover, induction upon fasting of ketone bodies and plasma FGF21 levels was blunted in *Atgl*<sup>adipo-/-</sup> mice (Figure 1A).

We performed gene expression profiling. Principal-component analysis (PCA) showed that differences in gene expression between *Atgl*<sup>adipo-/-</sup> and *Atgl*<sup>adipo+/+</sup> were observed in the fasting state (Figure S1A). Among the differentially expressed genes

(DEGs) between *Atgl*<sup>adipo-/-</sup> and *Atgl*<sup>adipo+/+</sup> (fold change [FC] > 2 and adjusted p value [adj.p] < 0.05), 99% were observed in fasted mice, while only 0.4% of the genes were differentially expressed in fed mice (Figure 1B). We performed hierarchical clustering on the DEGs with an FC > 2 and an adj.p < 0.05. The resulting heatmap identified seven clusters showing specific gene expression in response to fasting in the two genotypes (Figures 1C and 1D). Genes from clusters 4 and 7 were sensitive to fasting, but not dependent on *Atgl* expression in adipocytes (Figure 1D). The lack of adipocyte *Atgl* altered the expression of genes sensitive to fasting. We identified 1,073 upregulated genes (cluster 6) and 356 downregulated genes (cluster 2) specifically in fasted *Atgl*<sup>adipo-/-</sup> compared with *Atgl*<sup>adipo+/+</sup> mice. Genes from cluster 6 relate to dysregulation in cell cycle and apoptosis, enriched in *Hdac3*, *Creb1*, *Pparg*, *Trp53*, and *Nfkb1* targets (Figure 1E). The most upregulated genes are shown in Figure S1B. Genes from cluster 2, which were downregulated in the absence of adipocyte ATGL, are involved in metabolism. Furthermore, a cluster of 194 genes associated with circadian rhythm and lipid metabolism (cluster 1) were repressed by fasting, in an adipocyte ATGL-dependent manner (Figure 1E). Genes in cluster 5 showed increased expression in response to fasting in *Atgl*<sup>adipo+/+</sup>, but not *Atgl*<sup>adipo-/-</sup> mice. Gene enrichment analysis revealed that genes of this cluster are PPAR $\alpha$  targets related to fatty acid degradation and peroxisome biogenesis (Figures 1E and S1C). Genes expressed at higher levels in response to fasting in *Atgl*<sup>adipo+/+</sup> compared with *Atgl*<sup>adipo-/-</sup> mice include PPAR $\alpha$ -sensitive genes. Genes with the opposite profile include *Ddit4* and *Sesn1*, which are p53 target genes (Figure 1F). Accordingly, the expression of well-known PPAR $\alpha$  target genes was upregulated by fasting in *Atgl*<sup>adipo+/+</sup> mice but was low in the absence of adipocyte ATGL (Figure 1G). Similar profiles were observed for other PPAR $\alpha$  target genes (Figure S1D).

Together, these results reveal the important contribution of adipocyte ATGL to the regulation of the liver transcriptome in response to fasting. Further, it suggests a role of PPAR $\alpha$  in ATGL-dependent hepatic gene regulation.

### Hepatocyte PPAR $\alpha$ is critical for the fasting-induced adipose-ATGL-dependent effect on liver gene expression

To delineate the contribution of hepatocyte PPAR $\alpha$  to the fasting-induced adipocyte-ATGL-dependent regulation of hepatic gene expression, we compared the effect of adipocyte *Atgl* deletion with that of hepatocyte *Ppar $\alpha$*  deletion. We took advantage of published gene expression analysis from 24 h fasted

#### Figure 1. Adipose *Atgl* deficiency alters hepatic gene expression during fasting

*Atgl*<sup>adipo+/+</sup> and *Atgl*<sup>adipo-/-</sup> mice were fed *ad libitum* or fasted for 24 h (n = 6/group).

(A) Plasma FFAs, ketone bodies ( $\beta$ -hydroxybutyrate), and FGF21.

(B) Number of genes differentially expressed between *Atgl*<sup>adipo+/+</sup> and *Atgl*<sup>adipo-/-</sup> mice in fed and fasted states (FC > 2; adj.p < 0.05).

(C) Microarray experiment performed with liver samples. Hierarchical clustering shows the definition of seven gene clusters (FC > 2; adj.p < 0.05).

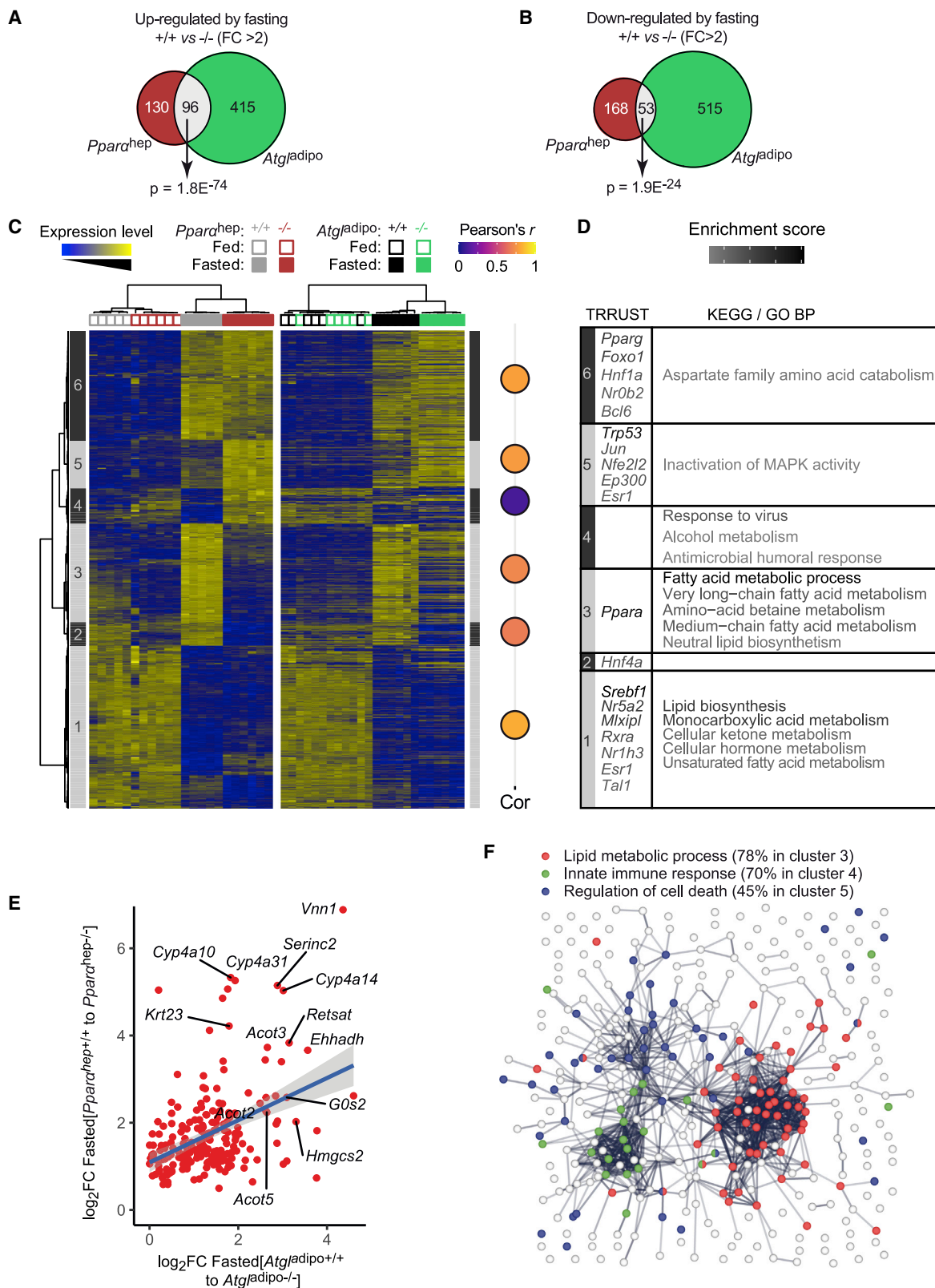
(D) Representation of the mean cluster profiles and number of genes in each cluster.

(E) Gene Ontology (GO) analysis and enrichment of transcription factors in each heatmap cluster.

(F) Volcano plot of differences in gene expression between *Atgl*<sup>adipo+/+</sup> and *Atgl*<sup>adipo-/-</sup> in fasting. The 20 most contrasted genes from clusters 5 and 6 are emphasized. The genes highlighted in red are PPAR $\alpha$  sensitive during fasting.

(G) Hepatic mRNA expression measured by qRT-PCR.

Results are the mean  $\pm$  SEM. #Fasting effect; \*genotype effect, and \*\*\* or ###p < 0.001. See also Figure S1.



(legend on next page)



hepatocyte-specific *Pparα* knockout mice (Régnier et al., 2018). Among the 17,508 probes ( $p < 0.05$ ) obtained in liver samples in both the PPAR $\alpha$  and ATGL experiments, we identified 511 probes corresponding to fasting-induced genes that were dependent on ATGL expression in adipocytes and 226 probes corresponding to fasting-induced genes dependent on PPAR $\alpha$  expression in hepatocytes (Figure 2A). Among them were 96 probes that shared a common pattern. We also found 568 probes and 221 probes corresponding to downregulated genes in fasted *Atgl*<sup>adipo+/+</sup> and fasted *Pparα*<sup>hep+/+</sup> mice, respectively, 53 of which were in common (Figure 2B). Hierarchical clustering performed on DEG ( $FC > 2$ ;  $p < 0.05$ ) in the *Pparα* deficiency model allowed the identification of six clusters with different patterns. These PPAR $\alpha$ -dependent changes in gene expression induced by fasting were analyzed in the adipose *Atgl*-deficient model. Most genes sensitive to both fasting and hepatocyte PPAR $\alpha$  were also dependent on adipocyte ATGL (Figure 2C). In contrast, genes in clusters 1 and 6 were sensitive to fasting but were not dependent on genotype. Furthermore, genes in cluster 2 were affected by hepatocyte *Pparα* and adipocyte *Atgl* deficiency in both the fed and fasted states; thus, these genes are not specifically regulated upon fasting. The expression of 281 fasting-induced genes in control *Atgl*<sup>adipo+/+</sup> and *Pparα*<sup>hep+/+</sup> mice (cluster 3) was not upregulated in both *Atgl*<sup>adipo-/-</sup> and *Pparα*<sup>hep-/-</sup> mice, suggesting that the expression of these genes was dependent on the presence of both ATGL in adipocytes and PPAR $\alpha$  in hepatocytes (Figure 2C). Among the genes dependent on adipocyte ATGL and hepatocyte PPAR $\alpha$  expression, many are PPAR $\alpha$  targets (Figures 2D and 2E). Gene network analysis confirmed the upregulation of genes involved in fatty acid metabolism and enriched in targets of PPAR $\alpha$  in response to fasting in control mice only, indicating a part played by both adipocyte ATGL and hepatocyte PPAR $\alpha$  (Figures 2F and S2). In contrast, cluster 5 included genes that were upregulated by fasting in the absence of both PPAR $\alpha$  in hepatocytes and ATGL in adipocytes (Figures 2C and S2). The main network includes genes involved in cell death (Figure 2F). Cluster 4 contained a small subset of genes that were upregulated in fasted *Pparα*<sup>hep-/-</sup> mice, but not in *Atgl*<sup>adipo-/-</sup> mice (Figure 2C), suggesting that these genes are repressed by PPAR $\alpha$ . Gene network analysis revealed that these genes are related to the innate immune response (Figures 2D and S2).

Altogether, these results reveal that the PPAR $\alpha$ -dependent response in the liver during fasting is dependent on adipocyte ATGL, suggesting that adipose-derived fatty acids are critical for hepatocyte PPAR $\alpha$  activity.

### Activation of $\beta_3$ -adrenergic signaling is sufficient to induce adipose ATGL-dependent PPAR $\alpha$ activity in hepatocytes

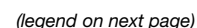
We next investigated the responses of *Atgl*<sup>adipo-/-</sup> and *Pparα*<sup>hep-/-</sup>-fed mice following induction of adipocyte lipolysis through activation of the  $\beta_3$ -adrenergic receptor using CL316243 (CL). Adipocyte *Atgl* deficiency reduced levels of FFAs, circulating ketone bodies, and FGF21 in response to CL (Figures 3A and 3B). In addition, the hepatic expression of PPAR $\alpha$  target genes was reduced in *Atgl*<sup>adipo-/-</sup> mice compared with *Atgl*<sup>adipo+/+</sup> mice, indicating that adipose ATGL is required for CL-induced PPAR $\alpha$  activity (Figure 3C). Hepatocyte *Pparα* deletion did not affect FFA levels following activation of  $\beta_3$ -adrenergic signaling (Figure 3D). However, similar to what was observed in *Atgl*<sup>adipo-/-</sup> mice, *Pparα*<sup>hep-/-</sup> mice exhibited an impaired  $\beta_3$ -adrenergic response in ketogenesis and FGF21 expression (Figures 3E and 3F). We evaluated hepatic gene expression patterns in CL-treated *Pparα*<sup>hep+/+</sup> and *Pparα*<sup>hep-/-</sup> mice. DEGs ( $FC > 2$ ; adj.p  $< 0.05$ ) were subjected to hierarchical clustering. The resulting heatmap highlights differences in hepatic gene expression between *Pparα*<sup>hep+/+</sup> and *Pparα*<sup>hep-/-</sup> mice in response to CL treatment (Figure 3G). We identified six clusters of genes (Figure 3H). Genes in cluster 1 and cluster 4 were regulated by CL, but not dependent on hepatocyte *Pparα*. Cluster 2 comprises 370 genes upregulated following  $\beta_3$ -adrenergic signaling activation in *Pparα*<sup>hep+/+</sup>, but not in *Pparα*<sup>hep-/-</sup> mice. These genes are associated with fatty acid metabolism and enriched in PPAR $\alpha$  targets. CL treatment decreased the expression of PPAR $\alpha$ -dependent genes (cluster 5) involved in steroid biosynthesis (Figures 3I and S3A). Conversely, the expression of a cluster of genes is sensitive to CL only in the absence of hepatocyte PPAR $\alpha$ . Cluster 6 included 218 genes that are involved in the response to unfolded proteins and inflammation (Figure 3I). Finally, the pathways repressed by CL in the absence of PPAR $\alpha$  in hepatocytes relate to fatty acid degradation and PPAR signaling (cluster 3; Figures 3I and S3B). Hepatic transcriptome analysis of CL-treated *Atgl*<sup>adipo+/+</sup> and *Atgl*<sup>adipo-/-</sup> also revealed that the absence of adipocyte ATGL had diverse effects on the response to CL (Figure S4). The main pathways induced by CL and dependent on adipocyte ATGL were related to fatty acid catabolism and peroxisome.

Taken together, these data show that the induction of adipocyte lipolysis induced PPAR $\alpha$ -dependent responses in the liver, even in the fed state. We tested whether insulin receptor (IR)-dependent signaling influences PPAR $\alpha$  activity using mice with hepatocyte-specific deletion of IR (Nemazany et al., 2015;

### Figure 2. Hepatocyte PPAR $\alpha$ is essential for adipose ATGL-dependent hepatic transcriptome in fasted mice

(A and B) Euler diagrams representing the number of probes corresponding to upregulated (A) and downregulated (B) genes upon fasting and differentially expressed ( $FC > 2$ ; adj.p  $< 0.05$ ) between *Atgl*<sup>adipo+/+</sup> and *Atgl*<sup>adipo-/-</sup> and/or *Pparα*<sup>hep+/+</sup> and *Pparα*<sup>hep-/-</sup>. (C) The first heatmap shows data from a microarray experiment performed with liver samples from *Pparα*<sup>hep+/+</sup> and *Pparα*<sup>hep-/-</sup> fed *ad libitum* or fasted ( $n = 6$ /group). Hierarchical clustering shows the definition of six gene clusters ( $FC > 2$ ; adj.p  $< 0.05$ ). The same gene clustering was applied to generate the second heatmap, which represents DEGs in the liver of *Atgl*<sup>adipo+/+</sup> and *Atgl*<sup>adipo-/-</sup> fed *ad libitum* or fasted ( $n = 6$ /group). Balloon plots on the right represent Pearson correlation coefficients for mean gene expression by experimental group in each cluster of both heatmaps. (D) GO analysis and enrichment of transcription factors in each heatmap cluster. BP, Biological Process; KEGG, Kyoto Encyclopedia of Genes and Genomes; MAPK, mitogen-activated protein kinase. (E) Correlation plot of expression levels of genes from cluster 3. (F) Gene network analysis of genes from clusters 3–5.

See also Figure S2.



Smati et al., 2020; Figures S5A and S5B). The expression of PPAR $\alpha$  target genes during fasting was not changed in absence of IR in hepatocytes (Figure S5C). In addition, deletion of IR in hepatocytes did not affect the decreased levels of plasma ketone bodies induced by refeeding (Figure S5D). Finally, we employed the gain-of-function model of chronically activated AKT signaling, the mouse mutant of hepatocyte-specific inactivation of phosphatase and tensin homolog (PTEN) protein (Horie et al., 2004; Patitucci et al., 2017). PTEN mutants showed normal ketogenesis during fasting (Figure S5E). These results suggest that cell-autonomous hepatocyte response to insulin is dispensable for inhibition of ketogenesis by feeding.

Previous study reported that FFAs activate PPAR $\beta/\delta$  (Sander-son et al., 2009). Therefore, we used mice with hepatocyte-specific *Ppar $\beta/\delta$*  deletion to analyze the metabolic responses following induction of lipolysis with CL. Compared with *Ppar $\beta/\delta$ <sup>hep+/+</sup>* mice, hepatocyte *Ppar $\beta/\delta$* -deficient (*Ppar $\beta/\delta$ <sup>hep-/-</sup>*) mice showed higher levels of plasma FFAs and ketone bodies in response to CL, whereas circulating FGF21 was unaffected by the absence of PPAR $\beta/\delta$  (Figures 3J and 3K). The hepatic expression of PPAR $\alpha$ -target genes in response to CL was increased in *Ppar $\beta/\delta$ <sup>hep-/-</sup>* mice compared with *Ppar $\beta/\delta$ <sup>hep+/+</sup>* mice, suggesting that PPAR $\beta/\delta$  may influence CL-induced PPAR $\alpha$  activity (Figure 3L). However, hepatocyte PPAR $\beta/\delta$  is dispensable for this  $\beta_3$ -adrenergic response dependent on WAT ATGL. Collectively, these results support a role for adipose lipolysis as a key signal for hepatocyte PPAR $\alpha$  activity.

### Hepatocyte PPAR $\alpha$ is required for BAT activation in response to activation of $\beta_3$ -adrenergic signaling

$\beta_3$ -adrenergic signaling not only induces triacylglycerol lipolysis in WAT but also activates thermogenesis in brown adipose tissue (BAT). Adipose ATGL is required to maintain body temperature during acute cold exposure (Haemmerle et al., 2006). We investigated the consequences of hepatocyte-specific *Ppar $\alpha$*  deletion on BAT activation in response to high-level lipolysis induced by combined CL treatment and fasting. Plasma FFA levels in response to CL were similar in the presence and absence of PPAR $\alpha$  in hepatocytes (Figure 4A). While blood glucose levels were decreased in both genotypes following CL treatment, insulin levels after CL-induced  $\beta_3$ -adrenergic signaling activation was

lower in *Ppar $\alpha$ <sup>hep-/-</sup>* mice compared with *Ppar $\alpha$ <sup>hep+/+</sup>* mice (Figure 4B). Plasma ketone bodies and FGF21 levels were reduced in fasted *Ppar $\alpha$ <sup>hep-/-</sup>* mice treated with  $\beta_3$ -adrenergic receptor agonist (Figure 4C). In agreement with Simcox et al. (2017), we found that CL decreased the plasma level of free carnitine and enhanced medium- and long-chain acylcarnitines (LCACs) levels. Compared with *Ppar $\alpha$ <sup>hep+/+</sup>* mice, *Ppar $\alpha$ <sup>hep-/-</sup>* mice exhibited higher levels of plasma LCACs (Figure 4D). CL-induced adipose lipolysis also influenced the expression of *Fgf21* and *In-hbe* dependent on hepatocyte PPAR $\alpha$  (Figure 4E). In contrast, other hepatokine expression, such as *Gdf15* and *Fst*, was induced in the liver of *Ppar $\alpha$ <sup>hep-/-</sup>* mice (Figure S6).

CL treatment reduced the number of BAT lipid droplets, indicating BAT activation, which was blunted in *Ppar $\alpha$ <sup>hep-/-</sup>* mice (Figure 4F). The deletion of hepatocyte *Ppar $\alpha$*  led to a reduction of *Ucp1* and *Elovl3* mRNA expression (Figure 4G), and UCP-1 protein expression in BAT was lower in *Ppar $\alpha$ <sup>hep-/-</sup>* mice (Figure 4H). Finally, acute cold exposure at 4°C resulted in hypothermia in *Ppar $\alpha$ <sup>hep-/-</sup>* mice compared with *Ppar $\alpha$ <sup>hep+/+</sup>* mice, indicating cold intolerance (Figure 4I).

During 24 h cold exposure in metabolic cages, food intake, locomotor activity, and body composition were similar in the two groups (Figures S7A–S7C), whereas energy expenditure (EE) and O<sub>2</sub> consumption (VO<sub>2</sub>) were increased in *Ppar $\alpha$ <sup>hep-/-</sup>* mice (Figures S7D and S7E). In addition, *Ppar $\alpha$ <sup>hep-/-</sup>* mice showed increased respiratory exchange rate (RER) (Figure S7F), suggesting a carbohydrate-oriented metabolism, and a lower rate of fatty acid oxidation during cold exposure (Figure S7F). In contrast, fasted *Ppar $\alpha$ <sup>hep-/-</sup>* mice showed no changes in EE, VO<sub>2</sub>, or RER (Figures S7G–S7I).

To investigate whether PPAR $\alpha$ -dependent BAT activation depends on FGF21, we challenged mice with hepatocyte-specific deletion of FGF21 with CL. Plasma levels of FFA, glucose, insulin, and circulating ketone bodies in response to CL were unaffected by the absence of hepatocyte FGF21 (Figures 4J–4L). Consistent with previous data showing that circulating FGF21 mostly originates from the liver (Markan et al., 2014), hepatocyte *Fgf21* deletion abolished increased level of plasma FGF21 in response to  $\beta_3$ -adrenergic signaling activation (Figure 4L). In addition, the deletion of *Fgf21* in hepatocytes did not affect the number of BAT lipid droplets (Figure 4M) and the expression of

### Figure 3. Hepatocyte PPAR $\alpha$ activity is induced upon activation of acute $\beta_3$ -adrenergic signaling

(A–C) *Atgl<sup>adipo+/+</sup>* and *Atgl<sup>adipo-/-</sup>* *ad libitum* fed mice received CL or vehicle (n = 6/group).

(A) Plasma FFA levels.

(B) Circulating levels of ketone bodies ( $\beta$ -hydroxybutyrate) and FGF21.

(C) Hepatic mRNA expression measured by qRT-PCR.

(D–I) *Ppar $\alpha$ <sup>hep+/+</sup>* and *Ppar $\alpha$ <sup>hep-/-</sup>* *ad libitum* fed mice received CL or vehicle (n = 8–9/group).

(D) Plasma FFA levels.

(E) Circulating levels of ketone bodies ( $\beta$ -hydroxybutyrate) and FGF21.

(F) Hepatic mRNA expression measured by qRT-PCR.

(G) Heatmap presenting data from a microarray experiment performed with liver samples (n = 6/group). Hierarchical clustering shows the definition of six gene clusters (FC > 2; adj.p ≤ 0.05).

(H) Representation of the mean cluster profiles and number of genes in each cluster.

(I) GO analysis and enrichment of transcription factors in each cluster.

(J–L) *Ppar $\beta$ <sup>hep+/+</sup>* and *Ppar $\beta$ <sup>hep-/-</sup>* *ad libitum* fed mice received CL or vehicle (n = 7–9/group).

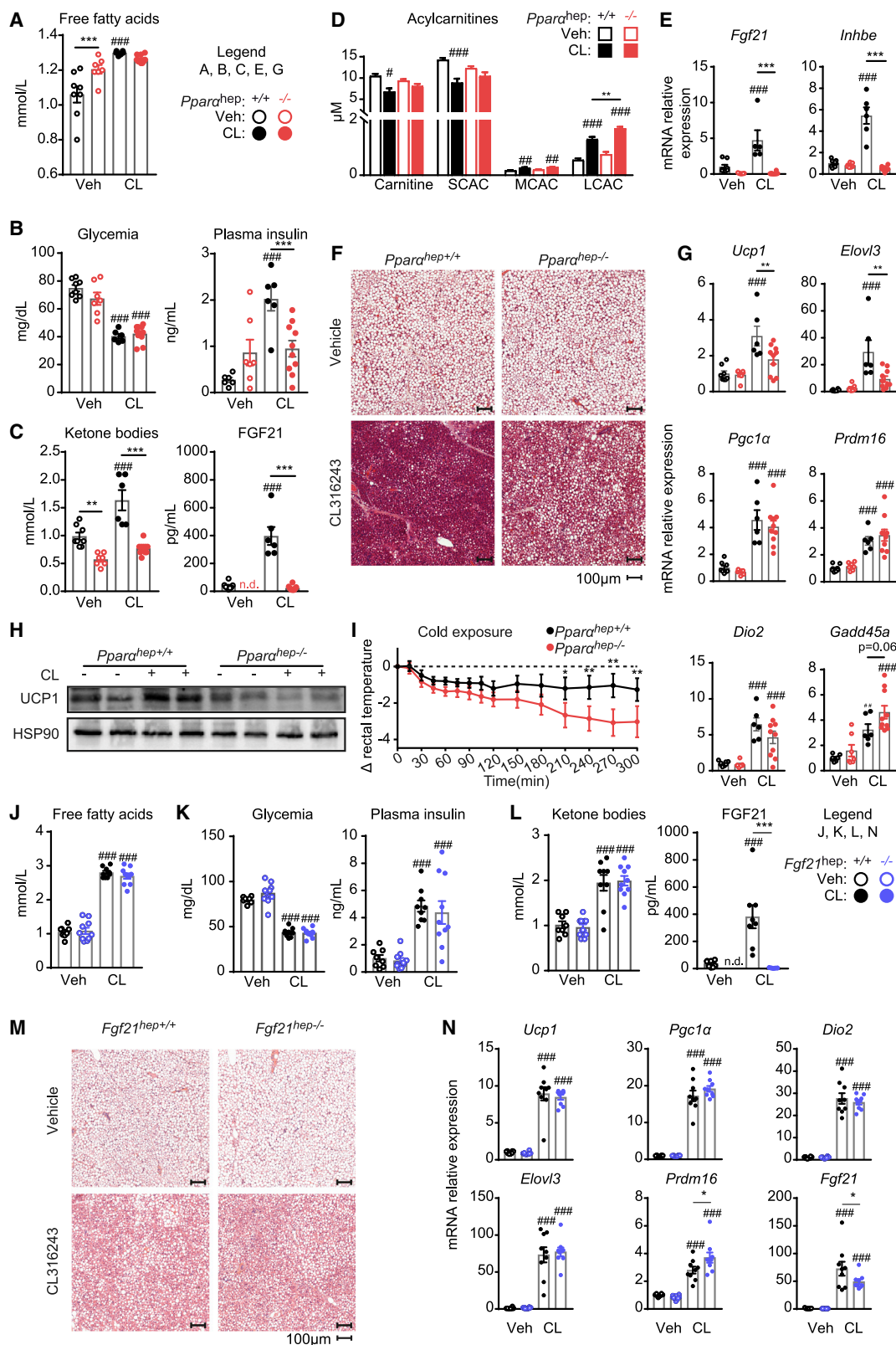
(J) Plasma FFA levels.

(K) Circulating levels of ketone bodies ( $\beta$ -hydroxybutyrate) and FGF21.

(L) Hepatic mRNA expression measured by qRT-PCR.

Results are the mean ± SEM. #CL effect; \*genotype effect; \* or #p < 0.05; \*\* or ##p < 0.01, and \*\*\* or ###p < 0.001. See also Figures S3 and S4.





(legend on next page)

BAT markers (Figure 4N), indicating that hepatocyte FGF21 is dispensable for BAT activation upon stimulation of  $\beta_3$ -adrenergic signaling.

These results demonstrated that hepatocyte PPAR $\alpha$  activity is required for the full activation of BAT. PPAR $\alpha$  activity in hepatocytes mediates the cross-talk between adipose tissues and the liver during lipolysis and thermogenesis through a mechanism that does not depend on FGF21.

## DISCUSSION

PPAR $\alpha$  is a regulator of hepatic lipid metabolism during fasting (Kersten et al., 1999; Montagner et al., 2016; Régnier et al., 2018). It is accepted that fatty acids derived from adipose tissue regulate hepatic gene expression (Jaeger et al., 2015). The first and rate-limiting step of adipose triacylglycerol lipolysis is catalyzed by ATGL. Global and adipocyte-specific *Atgl* deficiency in mice results in defective lipolysis (Haemmerle et al., 2006; Schoiswohl et al., 2015) and cold intolerance (Schreiber et al., 2017).

In this study, we used mouse models of selective deletion of *Atgl* in adipocytes and *Ppar $\alpha$*  in hepatocytes to investigate the contribution of ATGL-dependent lipolysis to PPAR $\alpha$  activity in the liver. Adipose tissue lipolysis was either induced by fasting or by  $\beta_3$ -adrenergic receptor stimulation.

Our data revealed the contribution of adipocyte ATGL to the metabolic response and liver gene expression during lipolysis. As previously reported (Jaeger et al., 2015; Schoiswohl et al., 2015), we found that ATGL-dependent lipolysis is required for fasting-induced ketone body and FGF21 production, two processes under the transcriptional control of PPAR $\alpha$  in hepatocytes (Badman et al., 2007; Inagaki et al., 2007; Montagner et al., 2016; Régnier et al., 2018). In addition, our analysis revealed that the genes most sensitive to *Atgl* deficiency included PPAR $\alpha$  target genes, such as *Fgf21*.

Comparison of gene expression profiles indicate that genes regulated by hepatocyte PPAR $\alpha$  in the liver during fasting also depend on ATGL-dependent lipolysis, suggesting that adipocyte ATGL-dependent lipolysis is required for PPAR $\alpha$ -dependent he-

patic gene expression and that together they orchestrate the fasting response in the liver. A recent study, using liver-specific deletion of *Atgl* in mice, has reported that hepatic ATGL is not required for the fasting-induced PPAR $\alpha$ -dependent responses in the liver, implying that adipocyte lipolysis-derived fatty acids are sufficient to activate PPAR $\alpha$  independent of hepatocyte lipolysis (Selen et al., 2021). We cannot exclude that adipose tissue lipolysis also activates other pathways, such as PPAR $\beta/\delta$ -dependent gene expression (Sanderson et al., 2009). However, our findings suggest that hepatic PPAR $\beta/\delta$  is dispensable for the effect of CL-induced adipose lipolysis on PPAR $\alpha$ -dependent regulation of gene expression, FGF21 production, and ketogenesis.

A set of genes related to immunity are upregulated by fasting in the absence of hepatocyte PPAR $\alpha$ , but not in the absence of adipocyte ATGL. This likely reflects the anti-inflammatory role of hepatocyte PPAR $\alpha$  (Paumelle et al., 2019; Pawlak et al., 2014).

Our work revealed that ATGL-dependent lipolysis repressed the hepatic expression of genes related to lipid metabolism and may be involved in the hepatic regulation of sterol regulatory element-binding proteins SREBP-1 and SREBP-2 (cluster 1; Figure 1E). This result is consistent with increased nuclear SREBP-1 levels in hepatocytes of *Atgl*<sup>adipo-/-</sup> mice after re-feeding (Wieser et al., 2020) and suggests that adipose lipolysis-derived fatty acids may suppress SREBP-1 activation in the liver.

We also identified a set of genes regulated by fasting in the absence of adipocyte ATGL, which suggests that they are either normally repressed by fatty acids derived from ATGL-dependent lipolysis or induced in the absence of fatty acids as a compensatory mechanism. They are mainly targets of p53, a transcription factor that regulates the expression of genes controlling cell proliferation and apoptosis and is frequently mutated in hepatocellular carcinoma (HCC) (Calderaro et al., 2017). Several lines of evidence indicate that p53 controls metabolic pathways (Lacroix et al., 2020). In mice, acute and hepatocyte-specific deletion of p53 leads to fasting hypoglycemia (Prokesch et al., 2017). In addition, p53 is necessary for fasting-mediated sensitization to therapeutic response of HCC-resistant models (Krstic et al.,

**Figure 4. Hepatocyte PPAR $\alpha$  deficiency causes reduced BAT activation and defective thermogenesis in response to  $\beta_3$ -adrenergic signaling activation**

(A–H) *Ppar $\alpha$* <sup>hep+/+</sup> and *Ppar $\alpha$* <sup>hep-/-</sup> mice were fasted for 10 h and then received CL or vehicle and were analyzed 6 h later (n = 6–10/group).

(A) Plasma FFA levels.

(B) Blood glucose and plasma insulin levels.

(C) Circulating levels of ketone bodies ( $\beta$ -hydroxybutyrate) and FGF21.

(D) Plasma levels of carnitine, short-chain acylcarnitines (SCACs) (C2–C5), medium-chain acylcarnitines (MCACs) (C6–C12), and long-chain acylcarnitines (LCACs) (C14–C18).

(E) Hepatic mRNA expression measured by qRT-PCR.

(F) Representative histological sections of BAT stained with H&E.

(G) mRNA relative expression in BAT measured by qRT-PCR.

(H) Representative UCP1 protein expression in BAT.

(I) Body temperature after a cold-tolerance test at 4°C.

(J–N) *Fgf21*<sup>hep+/+</sup> and *Fgf21*<sup>hep-/-</sup> mice were fasted and then received CL or vehicle (n = 9–10/group).

(J) Plasma FFA levels.

(K) Blood glucose and plasma insulin levels.

(L) Circulating levels of ketone bodies ( $\beta$ -hydroxybutyrate) and FGF21.

(M) Representative histological sections of BAT stained with H&E.

(N) mRNA expression measured in BAT by qRT-PCR.

Results are the mean  $\pm$  SEM. #CL effect, \*genotype effect, \* or #p < 0.05, \*\* or ##p < 0.01, and \*\*\* or ###p < 0.001. See also Figures S6 and S7.

2022). In the absence of ATGL, hepatic p53 may drive an adaptive response by coordinating cell cycle progression, apoptosis, and metabolism.

Furthermore, we observed that induction of lipolysis via acute CL treatment is sufficient to induce a PPAR $\alpha$ -dependent transcriptional response in fed animals. Thus, even when insulin is present, the PPAR $\alpha$ -dependent responses are induced upon adipose lipolysis stimulation. We also found that direct IR-dependent insulin signaling does not influence hepatocyte PPAR $\alpha$  activity. Although we cannot completely exclude negative regulation of PPAR $\alpha$  activity by the insulin/mTORC1 axis during feeding (Jo et al., 2015; Kim et al., 2012; Sengupta et al., 2010), our findings suggest that insulin-sensitive adipose tissue lipolysis acts as a key signal for hepatocyte PPAR $\alpha$  activation.

Another interesting finding is the effect of hepatocyte PPAR $\alpha$  on insulin following  $\beta_3$ -adrenergic receptor stimulation.  $\beta_3$ -adrenergic signaling activation promotes insulin secretion from pancreatic  $\beta$  cells despite the presence of hypoglycemia (Cypess et al., 2015). This response to CL requires the presence of  $\beta_3$ -adrenergic receptors in white adipocytes (Grujic et al., 1997). In addition, this process is blunted in mice with whole-body deletion of ATGL (MacPherson et al., 2014). It has been suggested that FFAs regulate insulin secretion through GPR40 (Itoh et al., 2003).

CL-mediated increase in plasma insulin levels depends on adipose lipolysis and is essential for the uptake of lipids by the BAT and for thermogenesis during  $\beta_3$ -adrenergic receptor stimulation (Heine et al., 2018). Here, we show that hepatocyte PPAR $\alpha$  influences insulin level, which suggests a cross-talk between the liver and the pancreas that involves PPAR $\alpha$ . Whether this effect is mediated by metabolites or through other hepatic signals remains to be investigated. We found that, upon activation of  $\beta_3$ -adrenergic signaling, hepatic *Ppar $\alpha$*  deficiency impairs expression of *Fgf21* and *Serp1b1*, two liver-derived proteins that influence  $\beta$  cell function (El Ouaamari et al., 2016; Wente et al., 2006). However, using mice with hepatocyte-specific deletion of *Fgf21*, we demonstrated that hepatic FGF21 does not influence insulin secretion induced by  $\beta_3$ -adrenergic activation.

Finally, our results reveal that PPAR $\alpha$  activity in hepatocytes influences BAT activation. Another study first identified the liver as an important tissue for thermogenesis regulation during cold exposure (Simcox et al., 2017). Simcox et al. showed that acylcarnitines generated by the liver through activation of HNF4 $\alpha$  in response to cold exposure are required to provide fuel for BAT thermogenesis. Here, we found that activation of hepatic PPAR $\alpha$  is also required for BAT activation. However, we did not observe differences in plasma acylcarnitine levels in *Ppar $\alpha$ <sup>hep-/-</sup>* mice compared with *Ppar $\alpha$ <sup>hep+/+</sup>* mice. Substrates for BAT activation include glucose (Hankir and Klingenspor, 2018), fatty acids derived from WAT lipolysis (Schreiber et al., 2017; Shin et al., 2017), circulating triglycerides (Heine et al., 2018), and acylcarnitines (Simcox et al., 2017). We did not find evidence that PPAR $\alpha$  influences these parameters. Other PPAR $\alpha$ -dependent metabolites include ketone bodies, which may also serve as an energy source to fuel thermogenesis (Mae-kubo et al., 1977).

We confirmed that hepatic PPAR $\alpha$  controls the hepatic expression of *Fgf21*, which influences BAT activity (Ameka et al., 2019; Fisher et al., 2012; Hondares et al., 2010). However, using mice with hepatocyte-specific deletion of *Fgf21*, we demonstrated that hepatic FGF21 is dispensable for such PPAR $\alpha$ -dependent activation of BAT in response to CL-induced lipolysis. We also identified activin E as a PPAR $\alpha$ -sensitive hepatokine likely to contribute to BAT activation (Hashimoto et al., 2018).

In conclusion, our study supports a dominant role for adipose ATGL in generating tissue-derived signal that triggers hepatocyte PPAR $\alpha$  activity and underscores the critical role of hepatic PPAR $\alpha$  in this adipose tissue to liver axis and in triggering BAT activation. Intact PPAR $\alpha$  activity in hepatocytes is required for the cross-talk between adipose tissues and the liver during fat mobilization.

### Limitations of the study

WAT ATGL is required for the regulation of liver gene expression. ATGL is the rate-limiting enzyme involved in triacylglycerol hydrolysis to produce diacylglycerol and FFA. It is possible that such lipids act as messengers to control the liver activity in response to lipolytic stimulus. A first limitation of our study is that we did not identify the ATGL-dependent signal that originates from the WAT to drive gene expression in the liver.

Hepatocyte PPAR $\alpha$  plays a part in the hepatic control of gene expression regulated by WAT lipolysis. However, another limitation is that we do not provide evidence for a direct genome recruitment and enhanced transcriptional activity of hepatocyte PPAR $\alpha$  in response to WAT lipolysis.

### STAR★METHODS

Detailed methods are provided in the online version of this paper and include the following:

- KEY RESOURCES TABLE
- RESOURCE AVAILABILITY
  - Lead contact
  - Material availability
  - Data and code availability
- EXPERIMENTAL MODEL AND SUBJECT DETAILS
  - Mice
- METHOD DETAILS
  - Fasting experiment and  $\beta_3$ -adrenergic receptor activation in the adipocyte Atgl-deficient mouse model
  - $\beta_3$ -adrenergic receptor activation and cold exposure in the hepatocyte *Ppar $\alpha$* -deficient mouse model
  - $\beta_3$ -adrenergic receptor activation in the hepatocyte *Ppar $\beta$* -deficient mouse model
  - $\beta_3$ -adrenergic receptor activation in the hepatocyte *Fgf21*-deficient mouse model
  - Fasting-refeeding experiment
  - Indirect calorimetry
  - Blood and tissue sampling
  - Blood glucose and plasma analysis
  - Gene expression
  - Histology

- UCP1 protein expression
- **QUANTIFICATION AND STATISTICAL ANALYSES**

## SUPPLEMENTAL INFORMATION

Supplemental information can be found online at <https://doi.org/10.1016/j.celrep.2022.110910>.

## ACKNOWLEDGMENTS

We thank all members of the EZOP staff, the GeT-Trix Genotoul facility, Aneplo and We-Met facilities for their help. A.F. was supported by AgreeSkills and Région Occitanie. B.T. was supported by FRM (FDM201906008682). C.A. was supported by the Boulos Foundation and FRM. Additional support was received by ANR (JCJC-16-CE14-0029) and ERC-2018-COG-MetaboSENS-819543 (G.P.); the German Research Foundation (DFG) (SCH 2546/5-1 to M.S.); the Leuchtturmprojekt/Flagship Project “Lipases and Lipid Signaling” (A.L.), funded by BioTechMed-Graz; and by P28882-B21 (G.S.), I3535, and P34899 (A.L.) by Austrian Science Fund (FWF). We acknowledge the support of the field of excellence “BioHealth” and NAWI Graz, Austria. This work was funded by ANR (ANR-17-CE14-0015) Hepadialogue (E.-Z.A., C.P., D.L., and H.G.), ANR (ANR-21-CE14-0079-01) Hepatologic (M.S., H.U., C.P., and H.G.), and by Région Occitanie (N.L., A.M., D.L., and H.G.).

## AUTHOR CONTRIBUTIONS

A.F. designed the project, performed experiments, analyzed the data, and wrote the paper. G.S., A.P., and M.R. contributed to designing experiments, performed experiments, and analyzed the data. C.W., S.S., T.F., Y.L., F.L., I.R., V.M., B.T., R.M., C.S., F.B., C.A., F.G., C.J., A.E., and P.D. contributed to experiments and data analysis. M.S., P.G., T.L., D.M., S.E.-S., L.G.-P., G.P., H.U., E.-Z.A., C.C.-G., C.P., W.W., N.L., A.M., and D.L. provided reagents and contributed to experiment design and supervision. A.L. and H.G. designed the project and analyzed the data. All authors revised the manuscript.

## DECLARATION OF INTERESTS

The authors declare no competing interests.

Received: February 4, 2022

Revised: March 22, 2022

Accepted: May 12, 2022

Published: June 7, 2022

## REFERENCES

- Ameka, M., Markan, K.R., Morgan, D.A., BonDurant, L.D., Idiga, S.O., Naber, M.C., Zhu, Z., Zingman, L.V., Grobe, J.L., Rahmouni, K., and Potthoff, M.J. (2019). Liver derived FGF21 maintains core body temperature during acute cold exposure. *Sci. Rep.* 9, 630. <https://doi.org/10.1038/s41598-018-37198-y>.
- Badman, M.K., Pissios, P., Kennedy, A.R., Koukos, G., Flier, J.S., and Maratos-Flier, E. (2007). Hepatic fibroblast growth factor 21 is regulated by PPAR $\alpha$  and is a key mediator of hepatic lipid metabolism in ketotic states. *Cell Metab.* 5, 426–437. <https://doi.org/10.1016/j.cmet.2007.05.002>.
- Benjamini, Y., and Hochberg, Y. (1995). Controlling the false discovery rate: a practical and powerful approach to multiple testing. *J. R. Stat. Soc. Ser. B* 57, 289–300. <https://doi.org/10.1111/j.2517-6161.1995.tb02031.x>.
- Calderaro, J., Couchy, G., Imbeaud, S., Amaddeo, G., Letouze, E., Blanc, J.F., Laurent, C., Hajji, Y., Azoulay, D., Bioulac-Sage, P., et al. (2017). Histological subtypes of hepatocellular carcinoma are related to gene mutations and molecular tumour classification. *J. Hepatol.* 67, 727–738. <https://doi.org/10.1016/j.jhep.2017.05.014>.
- Chace, D.H., Hillman, S.L., Van Hove, J.L.K., and Naylor, E.W. (1997). Rapid diagnosis of MCAD deficiency: quantitative analysis of octanoylcarnitine and other acylcarnitines in newborn blood spots by tandem mass spectrometry. *Clin. Chem.* 43, 2106–2113. <https://doi.org/10.1093/clinchem/43.11.2106>.
- Chakravarthy, M.V., Pan, Z., Zhu, Y., Tordjman, K., Schneider, J.G., Coleman, T., Turk, J., and Semenkovich, C.F. (2005). New hepatic fat activates PPAR $\alpha$  to maintain glucose, lipid, and cholesterol homeostasis. *Cell Metab.* 1, 309–322. <https://doi.org/10.1016/j.cmet.2005.04.002>.
- Chakravarthy, M.V., Lodhi, I.J., Yin, L., Malapaka, R.R.V., Xu, H.E., Turk, J., and Semenkovich, C.F. (2009). Identification of a physiologically relevant endogenous ligand for PPAR $\alpha$  in liver. *Cell* 138, 476–488. <https://doi.org/10.1016/j.cell.2009.05.036>.
- Chitru, C., Fischer, A.W., Farese, R.V., and Walther, T.C. (2020). Lipid droplets in Brown adipose tissue are dispensable for cold-induced thermogenesis. *Cell Rep.* 33, 108348. <https://doi.org/10.1016/j.celrep.2020.108348>.
- Cypess, A.M., Weiner, L.S., Roberts-Toler, C., Elia, E.F., Kessler, S.H., Kahn, P.A., English, J., Chatman, K., Trauger, S.A., Doria, A., and Kolodny, G. (2015). Activation of human brown adipose tissue by a  $\beta$ 3-adrenergic receptor agonist. *Cell Metab.* 21, 33–38. <https://doi.org/10.1016/j.cmet.2014.12.009>.
- Desvergne, B., and Wahli, W. (1999). Peroxisome proliferator-activated receptors: nuclear control of metabolism\*. *Endocr. Rev.* 20, 649–688. <https://doi.org/10.1210/er.20.5.649>.
- Fisher, F.M., Kleiner, S., Douris, N., Fox, E.C., Mepani, R.J., Verdeguer, F., Wu, J., Kharitonov, A., Flier, J.S., Maratos-Flier, E., and Spiegelman, B.M. (2012). FGF21 regulates PGC-1 $\alpha$  and browning of white adipose tissues in adaptive thermogenesis. *Genes Dev.* 26, 271–281. <https://doi.org/10.1101/gad.177857.111>.
- Goldstein, I., and Hager, G.L. (2015). Transcriptional and chromatin regulation during fasting – the genomic era. *Trends Endocrinol. Metab.* 26, 699–710. <https://doi.org/10.1016/j.tem.2015.09.005>.
- Grujic, D., Susulic, V.S., Harper, M.E., Himm-Hagen, J., Cunningham, B.A., Corkey, B.E., and Lowell, B.B. (1997).  $\beta$ 3-adrenergic receptors on white and brown adipocytes mediate  $\beta$ 3-selective agonist-induced effects on energy expenditure, insulin secretion, and food intake: a study using transgenic and gene knockout mice. *J. Biol. Chem.* 272, 17686–17693.
- Haemmerle, G., Lass, A., Zimmermann, R., Gorkiewicz, G., Meyer, C., Rozman, J., Heldmaier, G., Maier, R., Theussl, C., Eder, S., et al. (2006). Defective lipolysis and altered energy metabolism in mice lacking adipose triglyceride lipase. *Science* 312, 734–737. <https://doi.org/10.1126/science.1123965>.
- Han, M.S., Perry, R.J., Camporez, J.-P., Scherer, P.E., Shulman, G.I., Gao, G., and Davis, R.J. (2021). A feed-forward regulatory loop in adipose tissue promotes signaling by the hepatokine FGF21. *Genes Dev.* 35, 133–146. <https://doi.org/10.1101/gad.344556.120>.
- Hankir, M.K., and Klingenspor, M. (2018). Brown adipocyte glucose metabolism: a heated subject. *EMBO Rep.* 19, e46404. <https://doi.org/10.15252/embr.201846404>.
- Hashimoto, O., Funaba, M., Sekiyama, K., Doi, S., Shindo, D., Satoh, R., Itoi, H., Oiwa, H., Morita, M., Suzuki, C., et al. (2018). Activin E controls energy homeostasis in both Brown and white adipose tissues as a hepatokine. *Cell Rep.* 25, 1193–1203. <https://doi.org/10.1016/j.celrep.2018.10.008>.
- Heine, M., Fischer, A.W., Schlein, C., Jung, C., Straub, L.G., Gottschling, K., Mangels, N., Yuan, Y., Nilsson, S.K., Liebscher, G., et al. (2018). Lipolysis triggers a systemic insulin response essential for efficient energy replenishment of activated Brown adipose tissue in mice. *Cell Metab.* 28, 644–655.e4. <https://doi.org/10.1016/j.cmet.2018.06.020>.
- Hicks, S.C., Okrah, K., Paulson, J.N., Quackenbush, J., Irizarry, R.A., and Bravo, H.C. (2018). Smooth quantile normalization. *Biostatistics* 19, 185–198. <https://doi.org/10.1093/biostatistics/kxx028>.
- Hondares, E., Rosell, M., Gonzalez, F.J., Giral, M., Iglesias, R., and Villarroya, F. (2010). Hepatic FGF21 expression is induced at birth via PPAR $\alpha$  in response to milk intake and contributes to thermogenic activation of neonatal Brown fat. *Cell Metab.* 11, 206–212. <https://doi.org/10.1016/j.cmet.2010.02.001>.



- Horie, Y., Suzuki, A., Kataoka, E., Sasaki, T., Hamada, K., Sasaki, J., Mizuno, K., Hasegawa, G., Kishimoto, H., Iizuka, M., et al. (2004). Hepatocyte-specific Pten deficiency results in steatohepatitis and hepatocellular carcinomas. *J. Clin. Invest.* 113, 1774–1783. <https://doi.org/10.1172/jci20513>.
- Huber, W., Carey, V.J., Gentleman, R., Anders, S., Carlson, M., Carvalho, B.S., Bravo, H.C., Davis, S., Gatto, L., Girke, T., et al. (2015). Orchestrating high-throughput genomic analysis with Bioconductor. *Nat. Methods* 12, 115–121. <https://doi.org/10.1038/nmeth.3252>.
- Inagaki, T., Dutchak, P., Zhao, G., Ding, X., Gautron, L., Parameswara, V., Li, Y., Goetz, R., Mohammadi, M., Esser, V., et al. (2007). Endocrine regulation of the fasting response by PPAR $\alpha$ -mediated induction of fibroblast growth factor 21. *Cell Metab.* 5, 415–425. <https://doi.org/10.1016/j.cmet.2007.05.003>.
- Iroz, A., Montagner, A., Benhamed, F., Levavasseur, F., Polizzi, A., Anthony, E., Régnier, M., Fouché, E., Lukowicz, C., Cauzac, M., et al. (2017). A specific ChREBP and PPAR $\alpha$  cross-talk is required for the glucose-mediated FGF21 response. *Cell Rep.* 21, 403–416. <https://doi.org/10.1016/j.celrep.2017.09.065>.
- Itoh, Y., Kawamata, Y., Harada, M., Kobayashi, M., Fujii, R., Fukusumi, S., Ogi, K., Hosoya, M., Tanaka, Y., Uejima, H., et al. (2003). Free fatty acids regulate insulin secretion from pancreatic  $\beta$  cells through GPR40. *Nature* 422, 173–176. <https://doi.org/10.1038/nature01478>.
- Jaeger, D., Schoiswohl, G., Hofer, P., Schreiber, R., Schweiger, M., Eichmann, T.O., Pollak, N.M., Poecher, N., Grabner, G.F., Zierler, K.A., et al. (2015). Fasting-induced G0/G1 switch gene 2 and FGF21 expression in the liver are under regulation of adipose tissue derived fatty acids. *J. Hepatol.* 63, 437–445. <https://doi.org/10.1016/j.jhep.2015.02.035>.
- Jensen, T.L., Kiersgaard, M.K., Sørensen, D.B., and Mikkelsen, L.F. (2013). Fasting of mice: a review. *Lab. Anim.* 47, 225–240. <https://doi.org/10.1177/0023677213501659>.
- Jo, Y.S., Ryu, D., Maida, A., Wang, X., Evans, R.M., Schoonjans, K., and Auer, J. (2015). Phosphorylation of the nuclear receptor corepressor 1 by protein kinase B switches its corepressor targets in the liver in mice. *Hepatology* 62, 1606–1618. <https://doi.org/10.1002/hep.27907>.
- Kersten, S., Seydoux, J., Peters, J.M., Gonzalez, F.J., Desvergne, B., and Wahli, W. (1999). Peroxisome proliferator-activated receptor  $\alpha$  mediates the adaptive response to fasting. *J. Clin. Invest.* 103, 1489–1498. <https://doi.org/10.1172/jci6223>.
- Kim, K., Pyo, S., and Um, S.H. (2012). S6 kinase 2 deficiency enhances ketone body production and increases peroxisome proliferator-activated receptor alpha activity in the liver. *Hepatology* 55, 1727–1737. <https://doi.org/10.1002/hep.25537>.
- Kliwer, S.A., and Mangelsdorf, D.J. (2019). A dozen years of discovery: insights into the physiology and pharmacology of FGF21. *Cell Metab.* 29, 246–253. <https://doi.org/10.1016/j.cmet.2019.01.004>.
- Krstic, J., Reinisch, I., Schindlmaier, K., Galhuber, M., Riahi, Z., Berger, N., Kupper, N., Moyschewitz, E., Auer, M., Michenthaler, H., et al. (2022). Fasting improves therapeutic response in hepatocellular carcinoma through p53-dependent metabolic synergism. *Sci. Adv.* 8, eab2635. <https://doi.org/10.1126/sciadv.abh2635>.
- Lacroix, M., Riscal, R., Arena, G., Linares, L.K., and Le Cam, L. (2020). Metabolic functions of the tumor suppressor p53: implications in normal physiology, metabolic disorders, and cancer. *Mol. Metab.* 33, 2–22. <https://doi.org/10.1016/j.molmet.2019.10.002>.
- MacPherson, R.E.K., Castellani, L., Beaudoin, M.S., and Wright, D.C. (2014). Evidence for fatty acids mediating CL 316,243-induced reductions in blood glucose in mice. *Am. J. Physiol. Endocrinol. Metab.* 307, E563–E570. <https://doi.org/10.1152/ajpendo.00287.2014>.
- Maekubo, H., Moriya, K., and Hiroshige, T. (1977). Role of ketone bodies in nonshivering thermogenesis in cold acclimated rats. *J. Appl. Phys. Resp. Exerc. Physiol.* 42, 159–165. <https://doi.org/10.1152/jappl.1977.42.2.159>.
- Markan, K.R., Naber, M.C., Ameka, M.K., Andereg, M.D., Mangelsdorf, D.J., Kliwer, S.A., Mohammadi, M., and Potthoff, M.J. (2014). Circulating FGF21 is liver derived and enhances glucose uptake during refeeding and overfeeding. *Diabetes* 63, 4057–4063. <https://doi.org/10.2337/db14-0595>.
- Montagner, A., Polizzi, A., Fouché, E., Ducheix, S., Lippi, Y., Lasserre, F., Barquissau, V., Régnier, M., Lukowicz, C., Benhamed, F., et al. (2016). Liver PPAR $\alpha$  is crucial for whole-body fatty acid homeostasis and is protective against NAFLD. *Gut* 65, 1202–1214. <https://doi.org/10.1136/gutjnl-2015-310798>.
- Nemazany, I., Montagnac, G., Russell, R.C., Morzyglod, L., Burnol, A.-F., Guan, K.-L., Pende, M., and Panasyuk, G. (2015). Class III PI3K regulates organismal glucose homeostasis by providing negative feedback on hepatic insulin signalling. *Nat. Commun.* 6, 8283. <https://doi.org/10.1038/ncomms9283>.
- El Ouamari, A., Dirice, E., Gedeon, N., Hu, J., Zhou, J.Y., Shirakawa, J., Hou, L., Goodman, J., Karampelias, C., Qiang, G., et al. (2016). SerpinB1 promotes pancreatic  $\beta$  cell proliferation. *Cell Metab.* 23, 194–205. <https://doi.org/10.1016/j.cmet.2015.12.001>.
- Patitucci, C., Couchy, G., Bagattin, A., Cañeque, T., De Reyniès, A., Scoazec, J.Y., Rodriguez, R., Pontoglio, M., Zucman-Rossi, J., Pende, M., and Panasyuk, G. (2017). Hepatocyte nuclear factor 1 $\alpha$  suppresses steatosis-associated liver cancer by inhibiting PPAR $\gamma$  transcription. *J. Clin. Invest.* 127, 1873–1888. <https://doi.org/10.1172/jci90327>.
- Paumelle, R., Haas, J.T., Hennuyer, N., Baugé, E., Deleaye, Y., Mesotten, D., Langouche, L., Vanhoutte, J., Cudejko, C., Wouters, K., et al. (2019). Hepatic PPAR $\alpha$  is critical in the metabolic adaptation to sepsis. *J. Hepatol.* 70, 963–973. <https://doi.org/10.1016/j.jhep.2018.12.037>.
- Pawlak, M., Baugé, E., Bourguet, W., De Bosscher, K., Lalloyer, F., Tailleux, A., Lebherz, C., Lefebvre, P., and Staels, B. (2014). The transrepressive activity of peroxisome proliferator-activated receptor alpha is necessary and sufficient to prevent liver fibrosis in mice. *Hepatology* 60, 1593–1606. <https://doi.org/10.1002/hep.27297>.
- Polizzi, A., Fouché, E., Ducheix, S., Lasserre, F., Marmugi, A.P., Mselli-Lakhal, L., Loiseau, N., Wahli, W., Guillou, H., and Montagner, A. (2016). Hepatic fasting-induced PPAR $\alpha$  activity does not depend on essential fatty acids. *Int. J. Mol. Sci.* 17, 1624. <https://doi.org/10.3390/ijms17101624>.
- Prokesch, A., Graef, F.A., Madl, T., Kahlhofer, J., Heidenreich, S., Schumann, A., Moyschewitz, E., Pristovnik, P., Blaschitz, A., Knauer, M., et al. (2017). Liver p53 is stabilized upon starvation and required for amino acid catabolism and gluconeogenesis. *FASEB J.* 31, 732–742. <https://doi.org/10.1096/fj.201600845r>.
- Régnier, M., Polizzi, A., Lippi, Y., Fouché, E., Michel, G., Lukowicz, C., Smati, S., Marrot, A., Lasserre, F., Naylies, C., et al. (2018). Insights into the role of hepatocyte PPAR $\alpha$  activity in response to fasting. *Mol. Cell. Endocrinol.* 471, 75–88. <https://doi.org/10.1016/j.mce.2017.07.035>.
- Ritchie, M.E., Phipson, B., Wu, D., Hu, Y., Law, C.W., Shi, W., and Smyth, G.K. (2015). Limma powers differential expression analyses for RNA-sequencing and microarray studies. *Nucleic Acids Res.* 43, e47. <https://doi.org/10.1093/nar/gkv007>.
- Ruijter, J.M., Ramakers, C., Hoogaars, W.M.H., Karlen, Y., Bakker, O., van den Hoff, M.J.B., and Moorman, A.F.M. (2009). Amplification efficiency: linking baseline and bias in the analysis of quantitative PCR data. *Nucleic Acids Res.* 37, e45. <https://doi.org/10.1093/nar/gkp045>.
- Sanderson, L.M., Degenhardt, T., Koppen, A., Kalkhoven, E., Desvergne, B., Müller, M., and Kersten, S. (2009). Peroxisome proliferator-activated receptor  $\beta/\delta$  (PPAR $\beta/\delta$ ) but not PPAR $\alpha$  serves as a plasma free fatty acid sensor in liver. *Mol. Cell Biol.* 29, 6257–6267. <https://doi.org/10.1128/mcb.00370-09>.
- Schoiswohl, G., Stefanovic-Racic, M., Menke, M.N., Wills, R.C., Surlow, B.A., Basantani, M.K., Sitnick, M.T., Cai, L., Yazbeck, C.F., Stolz, D.B., et al. (2015). Impact of reduced ATGL-mediated adipocyte lipolysis on obesity-associated insulin resistance and inflammation in male mice. *Endocrinology* 156, 3610–3624. <https://doi.org/10.1210/en.2015-1322>.
- Schreiber, R., Diwoky, C., Schoiswohl, G., Feiler, U., Wongsiriroj, N., Abdellatif, M., Kolb, D., Hoeks, J., Kershaw, E.E., Sedej, S., et al. (2017). Cold-induced thermogenesis depends on ATGL-mediated lipolysis in cardiac muscle, but



not Brown adipose tissue. *Cell Metab.* 26, 753–763.e7. <https://doi.org/10.1016/j.cmet.2017.09.004>.

Schuler, M., Ali, F., Chambon, C., Duteil, D., Bornert, J.M., Tardivel, A., Desvergne, B., Wahli, W., Chambon, P., and Metzger, D. (2006). PGC1 $\alpha$  expression is controlled in skeletal muscles by PPAR $\beta$ , whose ablation results in fiber-type switching, obesity, and type 2 diabetes. *Cell Metab.* 4, 407–414. <https://doi.org/10.1016/j.cmet.2006.10.003>.

Selen, E.S., Choi, J., and Wolfgang, M.J. (2021). Discordant hepatic fatty acid oxidation and triglyceride hydrolysis leads to liver disease. *JCI Insight* 6, e135626. <https://doi.org/10.1172/jci.insight.135626>.

Sengupta, S., Peterson, T.R., Laplante, M., Oh, S., and Sabatini, D.M. (2010). mTORC1 controls fasting-induced ketogenesis and its modulation by ageing. *Nature* 468, 1100–1104. <https://doi.org/10.1038/nature09584>.

Shin, H., Ma, Y., Chanturiya, T., Cao, Q., Wang, Y., Kadegowda, A.K.G., Jackson, R., Rumore, D., Xue, B., Shi, H., et al. (2017). Lipolysis in Brown adipocytes is not essential for cold-induced thermogenesis in mice. *Cell Metab.* 26, 764–777.e5. <https://doi.org/10.1016/j.cmet.2017.09.002>.

Simcox, J., Geoghegan, G., Maschek, J.A., Bensard, C.L., Pasquali, M., Miao, R., Lee, S., Jiang, L., Huck, I., Kershaw, E.E., et al. (2017). Global analysis of plasma lipids identifies liver-derived acylcarnitines as a fuel source for Brown fat thermogenesis. *Cell Metab.* 26, 509–522.e6. <https://doi.org/10.1016/j.cmet.2017.08.006>.

Smati, S., Régnier, M., Fougeray, T., Polizzi, A., Fougerat, A., Lasserre, F., Lukowicz, C., Tramunt, B., Guillaume, M., Burnol, A.F., et al. (2020). Regulation of hepatokine gene expression in response to fasting and feeding: influence of PPAR- $\alpha$  and insulin-dependent signalling in hepatocytes. *Diabetes Metab.* 46, 129–136. <https://doi.org/10.1016/j.diabet.2019.05.005>.

Szklarczyk, D., Gable, A.L., Lyon, D., Junge, A., Wyder, S., Huerta-Cepas, J., Simonovic, M., Doncheva, N.T., Morris, J.H., Bork, P., et al. (2019). STRING v11: protein–protein association networks with increased coverage, supporting functional discovery in genome-wide experimental datasets. *Nucleic Acids Res.* 47, D607–D613. <https://doi.org/10.1093/nar/gky1131>.

Tuomi, J.M., Voorbraak, F., Jones, D.L., and Ruijter, J.M. (2010). Bias in the Cq value observed with hydrolysis probe based quantitative PCR can be corrected with the estimated PCR efficiency value. *Methods* 50, 313–322. <https://doi.org/10.1016/j.ymeth.2010.02.003>.

Wente, W., Efanov, A.M., Brenner, M., Kharitonov, A., Köster, A., Sandusky, G.E., Sewing, S., Treinies, I., Zitzer, H., and Gromada, J. (2006). Fibroblast growth factor-21 improves pancreatic beta-cell function and survival by activation of extracellular signal-regulated kinase 1/2 and Akt signaling pathways. *Diabetes* 55, 2470–2478. <https://doi.org/10.2337/db05-1435>.

Wickham. (2019). Welcome to the Tidyverse. *Journal of Open Source Software* 4, 1686. <https://doi.org/10.21105/joss.01686>.

Wieser, B.I., Peña De La Sancha, P., Schauer, S., Reicher, H., Sattler, W., Breinbauer, R., Schweiger, M., Espenshade, P.J., Zechner, R., Hoefler, G., et al. (2020). Adipose triglyceride lipase is needed for homeostatic control of Sterol element-binding protein-1c driven hepatic lipogenesis. Preprint at bioRxiv. <https://doi.org/10.1101/2020.11.02.363440>.

Zhou, Y., Zhou, B., Pache, L., Chang, M., Khodabakhshi, A.H., Tanaseichuk, O., Benner, C., and Chanda, S.K. (2019). Metascape provides a biologist-oriented resource for the analysis of systems-level datasets. *Nat. Commun.* 10, 1523. <https://doi.org/10.1038/s41467-019-09234-6>.

## STAR★METHODS

### KEY RESOURCES TABLE

REAGENT or RESOURCE	SOURCE	IDENTIFIER
<b>Antibodies</b>		
UCP1	Abcam	Cat# ab10983, RRID:AB_2241462
Hsp90 (C45G5)	Cell Signaling	Cat# 4877, RRID:AB_2233307
Insulin R $\beta$ (CT-3)	Santa Cruz Biotechnology	Cat# sc-57342, RRID:AB_784102
Phospho-Akt (Ser473) (193H12)	Cell Signaling	Cat# 4058, RRID:AB_331168
Akt (pan) (C67E7)	Cell Signaling	Cat# 4691, RRID:AB_915783
$\beta$ -Actin (13E5)	Cell Signaling	Cat# 4970, RRID:AB_2223172
<b>Chemicals, peptides, and recombinant proteins</b>		
CL 316,243	Sigma-Aldrich	Cat# C5976
Tamoxifen Free Base	MP Biomedicals	Cat #156738
Clarity ECL	Bio-Rad	Cat #170-5060
SYBR Green	Applied Biosystems	Cat #4367659
TRIZOL Reagent	Invitrogen	Cat #TR118
<b>Critical commercial assays</b>		
FGF21 ELISA kit	Sigma-Aldrich	Cat# EZRMFGF21-26K
Sureprint G3 Mouse G v2 microarrays	Agilent Technologies	N/A
Hot star Taq DNA Polymerase	Qiagen	Cat #203605
High Capacity cDNA RT kit	ThermoFisher	Cat #4368813
BCA Protein Assay kit	ThermoFisher	Cat #23227
<b>Deposited data</b>		
Microarray data	<a href="#">Régner et al. (2018)</a>	GEO: GSE96559
Microarray data	This paper	GEO: GSE165699
Microarray data	This paper	GEO: GSE165558
<b>Experimental models: Organisms/strains</b>		
Mouse: Albumin-Cre <sup>-/-</sup> Ppar $\alpha$ <sup>flox/flox</sup>	<a href="#">Montagner et al. (2016)</a>	N/A
Mouse: Albumin-Cre <sup>+/-</sup> Ppar $\alpha$ <sup>flox/flox</sup>	<a href="#">Montagner et al. (2016)</a>	N/A
Mouse: Adiponectin-Cre <sup>-/-</sup> Atgl <sup>flox/flox</sup>	<a href="#">Schoiswohl et al. (2015)</a>	N/A
Mouse: Adiponectin-Cre <sup>+/-</sup> Atgl <sup>flox/flox</sup>	<a href="#">Schoiswohl et al. (2015)</a>	N/A
Mouse: Albumin-Cre <sup>-/-</sup> Fgf21 <sup>flox/flox</sup>	This paper	N/A
Mouse: Albumin-Cre <sup>+/-</sup> Fgf21 <sup>flox/flox</sup>	This paper	N/A
Mouse: Transthyretin-Cre <sup>-/-</sup> IR <sup>flox/flox</sup>	<a href="#">Nemazany et al. (2015)</a> <a href="#">Smati et al. (2020)</a>	N/A
Mouse: Transthyretin-Cre <sup>+/-</sup> IR <sup>flox/flox</sup>	<a href="#">Nemazany et al. (2015)</a> <a href="#">Smati et al. (2020)</a>	N/A
Mouse: Albumin-Cre <sup>-/-</sup> Pten <sup>flox/flox</sup>	<a href="#">Horie et al. (2004)</a> <a href="#">Patitucci et al. (2017)</a>	N/A
Mouse: Albumin-Cre <sup>+/-</sup> Pten <sup>flox/flox</sup>	<a href="#">Horie et al. (2004)</a> <a href="#">Patitucci et al. (2017)</a>	N/A
Mouse: Albumin-Cre <sup>-/-</sup> Ppar $\beta$ <sup>flox/flox</sup>	<a href="#">Schuler et al. (2006)</a>	N/A
Mouse: Albumin-Cre <sup>+/-</sup> Ppar $\beta$ <sup>flox/flox</sup>	This paper	N/A
<b>Oligonucleotides</b>		
Oligonucleotide sequences are listed in <a href="#">Table S1</a>	This paper	N/A
<b>Software and algorithms</b>		
LinRegPCR (v2017.1)	<a href="#">Ruijter et al. (2009)</a>	<a href="http://LinRegPCR.nl">http://LinRegPCR.nl</a>
GraphPad Prism (version 7.00)	GraphPad	<a href="https://www.graphpad.com">https://www.graphpad.com</a>
Metascape	<a href="#">Zhou et al. (2019)</a>	<a href="http://metascape.org">http://metascape.org</a>

(Continued on next page)

**Continued**

REAGENT or RESOURCE	SOURCE	IDENTIFIER
R (v4.1.2)	R Core Team (2021)	<a href="https://www.R-project.org/">https://www.R-project.org/</a>
Rstudio(v2021.09.0)	RStudio, PBC	<a href="https://www.rstudio.com/">https://www.rstudio.com/</a>
Bioconductor	Huber et al. (2015)	<a href="https://bioconductor.org/">https://bioconductor.org/</a>
tidyverse (v1.3.1)	Wickham (2019) <a href="https://doi.org/10.21105/joss.01686">https://doi.org/10.21105/joss.01686</a>	<a href="https://cran.r-project.org/package=tidyverse">https://cran.r-project.org/package=tidyverse</a>
pheatmap (v1.0.12)	Raivo Kolde (2019)	<a href="https://cran.r-project.org/package=pheatmap">https://cran.r-project.org/package=pheatmap</a>
Illustrator(v26.1)	Adobe	<a href="http://www.adobe.com/illustrator">www.adobe.com/illustrator</a>
limma(v3.48.3)	Ritchie et al. (2015)	<a href="https://bioconductor.org/packages/release/bioc/html/limma.html">https://bioconductor.org/packages/release/bioc/html/limma.html</a>
Scan Control A.8.5.1	Agilent	<a href="https://www.agilent.com/">https://www.agilent.com/</a>
Feature Extraction software v10.10.1.1	Agilent	<a href="https://www.agilent.com/">https://www.agilent.com/</a>
AriaMx (v1.8)	Agilent	<a href="https://www.agilent.com/">https://www.agilent.com/</a>

## RESOURCE AVAILABILITY

### Lead contact

Further information and requests for resources and reagents should be directed to and will be fulfilled by the lead contact, Hervé Guillou ([hervé.guillou@inrae.fr](mailto:hervé.guillou@inrae.fr)).

### Material availability

This study did not generate new reagents. Mouse lines for this study are available from the [lead contact](#) with a completed material transfer agreement.

### Data and code availability

- Microarray data have been deposited at GEO and are publicly available as of the date of publication. Accession numbers are listed in the [Key resources table](#). All data reported in this paper will be shared by the [lead contact](#) upon request.
- This paper does not report original code.
- Any additional information required to reanalyze the data reported in this paper is available from the [lead contact](#) upon request.

## EXPERIMENTAL MODEL AND SUBJECT DETAILS

### Mice

*In vivo* studies were performed in compliance with the European guidelines for the use and care of laboratory animals, and approved by an independent ethics committee under the authorization numbers 16432-2018081010184501, 31741-2021052011598985, 14005-2018030917086471 and 17430-2018110611093660, and by the Austrian Federal Ministry for Science, Research, and Economy (protocol number GZ: 39/9-4/75 ex 2017/18). All mice were housed at 21–23°C on a 12-h light (ZT0–ZT12)/12-h dark (ZT12–ZT24) cycle and had free access to the standard rodent diet (Safe 04 U8220G10R) and tap water. ZT stands for Zeitgeber time; ZT0 is defined as the time when the lights are turned on. All mice used in this study were males and were sacrificed at ZT16, unless stated otherwise. All experiments were performed in 12–16 week-old mice.

*Pparα* hepatocyte-specific knockout (*Pparα*<sup>hep−/−</sup>) mice were generated at INRAE's rodent facility (Toulouse, France) by mating the floxed-*Pparα* mouse strain with C57BL/6J albumin-Cre transgenic mice, as described previously ([Montagner et al., 2016](#)), to obtain albumin-Cre<sup>+/−</sup>*Pparα*<sup>flox/flox</sup> mice. Albumin-Cre<sup>−/−</sup>*Pparα*<sup>flox/flox</sup> (*Pparα*<sup>hep+/+</sup>) littermates were used as controls. Genotyping was performed using an established protocol ([Montagner et al., 2016](#)).

Adipocyte-specific *Atgl* knockout (*Atgl*<sup>adipo−/−</sup>) mice were bred at the animal facility of the University of Graz. They were originally generated at the animal facility of the University of Pittsburgh by mating the floxed-*Atgl* mouse strain with adiponectin-Cre mice, as described previously ([Schoiswohl et al., 2015](#)), to obtain adiponectin-Cre<sup>+/−</sup>*Atgl*<sup>flox/flox</sup> mice. Adiponectin-Cre<sup>−/−</sup>*Atgl*<sup>flox/flox</sup> mice (*Atgl*<sup>adipo+/+</sup>) were used as controls.

*Pparβ* hepatocyte-specific knockout (*Pparβ*<sup>hep−/−</sup>) mice were generated at INRAE's rodent facility (Toulouse, France) by mating the floxed-*Pparβ* mouse strain ([Schuler et al., 2006](#)) with C57BL/6J albumin-Cre transgenic mice, to obtain albumin-Cre<sup>+/−</sup>*Pparβ*<sup>flox/flox</sup> mice. Albumin-Cre<sup>−/−</sup>*Pparβ*<sup>flox/flox</sup> (*Pparβ*<sup>hep+/+</sup>) littermates were used as controls.

*Fgf21* hepatocyte-specific knockout (*Fgf21*<sup>hep-/-</sup>) mice were generated at INRAE's rodent facility (Toulouse, France) by mating the floxed-*Fgf21* mouse strain (B6.129S6(SJL)*Fgf21* < tm1.2Djm>/J provided by The Jackson Laboratory) with C57BL/6J albumin-Cre transgenic mice, to obtain albumin-Cre<sup>+/+</sup>-*Fgf21*<sup>flox/flox</sup> mice. Albumin-Cre<sup>-/-</sup>-*Fgf21*<sup>flox/flox</sup> (*Fgf21*<sup>hep+/+</sup>) littermates were used as controls.

Insulin receptor hepatocyte-specific knockout (*IR*<sup>hep-/-</sup>) mice: Animals carrying LoxP sites flanking the fourth exon of the *IR* gene (*IR*<sup>lox/lox</sup> stock number: 006955; Jackson Laboratory, Bar Harbor, ME, USA) were intercrossed with C57BL/6J mice, which specifically express Cre recombinase in the liver under the transthyretin promoter (TTR-CreTam mice), as previously described (Nemazany et al., 2015; Smati et al., 2020). At the age of 8 weeks, males *IR*<sup>hep-/-</sup> (*IR*<sup>floxed/floxed/TTR-CreTam+/+</sup>) and *IR*<sup>hep+/+</sup> (*IR*<sup>floxed/floxed/TTR-CreTam-/-</sup>) mice received tamoxifen (Tamoxifen Free Base, MP Biomedicals) by intraperitoneal injection (1.5mg/kg) during three consecutive days, to induce deletion of hepatocyte Insulin receptor. Experiments started two weeks after the last tamoxifen injection.

PTEN hepatocyte-specific knockout (*PTEN*<sup>hep-/-</sup>) mice: *Pten*<sup>flox/flox</sup> mice were mated to AlbCre transgenic mice (C57BL/6J background; The Jackson Laboratory, Bar Harbor, Maine, USA), in which expression of Cre is controlled by the promoter of the hepatocyte-specific gene Albumin, as previously described (Horie et al., 2004; Patitucci et al., 2017).

## METHOD DETAILS

### Fasting experiment and $\beta_3$ -adrenergic receptor activation in the adipocyte *Atgl*-deficient mouse model

Six 12-week-old mice were fed *ad libitum* or fasted for 24 h (starting at ZT16). For  $\beta_3$ -adrenergic receptor activation, 12-week-old mice were transferred in a ventilated cabinet at the specific temperature of 30°C (thermoneutrality) 2 weeks before experiments. Mice were fed *ad libitum* and given CL316243 (3 mg/kg body weight; Sigma Aldrich) or vehicle (0.5% carboxymethylcellulose in sterilized water) by gavage at ZT10 and sacrificed at ZT16 (n = 6/genotype/experimental condition).

Plasma FFA levels and PPAR $\alpha$  activity are increased after 24 h of fasting (Jensen et al., 2013; Montagner et al., 2016). Moreover hepatic PPAR $\alpha$  expression as well as its activity are circadian and peak at ZT16 (Montagner et al., 2016). Therefore, we chose here to fast mice for 24 h starting at ZT16.

### $\beta_3$ -adrenergic receptor activation and cold exposure in the hepatocyte *Ppar $\alpha$* -deficient mouse model

Twelve-week-old mice were transferred in a ventilated cabinet at the specific temperature of 30°C (thermoneutrality) 2 weeks before experiments. Mice were fed *ad libitum* or fasted at ZT0 and given CL316243 (3 mg/kg body weight; Sigma Aldrich) or vehicle (0.5% carboxymethylcellulose in sterilized water) by gavage at ZT10 and sacrificed at ZT16 (n = 6–10/genotype/experimental condition). For cold exposure, mice were single-housed without nesting material and had free access to food and water. Mice were transferred to 4°C for 5 h. Body temperature was taken every 15 min during the first hour, every 30 min during the second hour, then every hour with a RET-3 rectal probe (Physitemp) using a digital thermometer (Bioseb) (n = 8/genotype).

### $\beta_3$ -adrenergic receptor activation in the hepatocyte *Ppar $\beta$* -deficient mouse model

Sixteen-week-old mice were transferred in a ventilated cabinet at the specific temperature of 30°C (thermoneutrality) 2 weeks before experiments. Mice were fed *ad libitum* and given CL316243 (3 mg/kg body weight; Sigma Aldrich) or vehicle (0.5% carboxymethylcellulose in sterilized water) by gavage at ZT18 and sacrificed at ZT24 (n = 7–9/genotype/experimental condition).

### $\beta_3$ -adrenergic receptor activation in the hepatocyte *Fgf21*-deficient mouse model

Fourteen-week-old mice were transferred in a ventilated cabinet at the specific temperature of 30°C (thermoneutrality) 2 weeks before experiments. Mice were fasted at ZT0 and given CL316243 (3 mg/kg body weight; Sigma Aldrich) or vehicle (0.5% carboxymethylcellulose in sterilized water) by gavage at ZT10 and sacrificed at ZT16 (n = 8–10/genotype/experimental condition).

### Fasting-refeeding experiment

Twelve-week-old *IR*<sup>hep+/+</sup> and *IR*<sup>hep-/-</sup> mice were fasted for 12 h (starting at ZT12) or fasted for 12 h (from ZT12) and then re-fed *ad libitum* until sacrifice (n = 6 mice/genotype/experimental condition).

### Indirect calorimetry

All animals were individually housed in a cage with lights on from 8 a.m. to 8 p.m. and an ambient temperature of 22 ± 0.5 or 7°C for cold exposure. Mice were acclimated to their calorimetric cages for 48 h before experimental measurements. After baseline recordings for 3 days, mice were either fasted for 24 h or fed *ad libitum* and exposed to 7°C for 24 h. Data were collected every 15 min. Total energy expenditure (kcal/h), oxygen consumption and carbon dioxide production (VO<sub>2</sub> and VCO<sub>2</sub>, where V is the volume), respiratory exchange rate (RER = VCO<sub>2</sub>/VO<sub>2</sub>), food intake (g), and locomotor activity (beam breaks/h) were measured using calorimetric cages with bedding, food and water *ad libitum* (Labmaster, TSE Systems GmbH, Bad Homburg, Germany). Animals were monitored for body weight and composition at the beginning and end of the experiment. Data analysis was carried out with Excel XP using extracted raw values of VO<sub>2</sub> consumption, VCO<sub>2</sub> production (mL/h), and energy expenditure (kcal/h). Subsequently, each value was expressed as a function of total lean tissue mass extracted from the EchoMRI analysis.

### Blood and tissue sampling

Prior to sacrifice, blood was collected into EDTA-coated tubes (Sarstedt, K3E tubes) from the submandibular vein. Plasma was prepared by centrifugation (1500 g, 15 min, 4°C) and stored at –80°C. Following sacrifice by cervical dislocation, the liver and the BAT were removed, weighed, and prepared for histology, or snap frozen in liquid nitrogen and stored at –80°C until use.

### Blood glucose and plasma analysis

Free fatty acids (FFAs) were determined from plasma samples using a COBASMIRA + biochemical analyzer (Anexplo facility, Toulouse, France). Plasma insulin concentration was measured using the Insulin Mouse Serum Assay HTRF Kit (Cisbio) (WE-MET in Toulouse). Blood glucose was measured with an Accu-Chek Guide glucometer (Roche Diagnostics).  $\beta$ -Hydroxybutyrate was measured with Optium  $\beta$ -ketone test strips that carried Optium Xceed sensors (Abbott Diabetes Care). Plasma FGF21 was assayed using the rat/mouse FGF21 ELISA kit (Sigma) according to the manufacturer's instructions.

Free carnitine and acylcarnitines were measured from plasma (10  $\mu$ L) spotted on filter membranes (Protein Saver 903 cards; Whatman), dried, and then treated as reported (Chace et al., 1997). Briefly, acylcarnitines were derivatized to their butyl esters and treated with the reagents of the NeoGram MSMS-AAAC kit (PerkinElmer). Their analysis was carried out on a Waters 2795/Quattro Micro AP liquid chromatography–tandem mass spectrometer (Waters, Milford, MA).

### Gene expression

Total cellular RNA was extracted from liver and BAT samples using TRIzol reagent (Invitrogen). RNA was quantified using a NanoDrop (Nanophotometer N60, Implen). Two micrograms of total RNA were reverse transcribed using the High-Capacity cDNA Reverse Transcription Kit (Applied Biosystems) for real-time quantitative polymerase chain reaction (qPCR) analyses. Primers for Sybr Green assays are presented in Table S1. Amplifications were performed on an ABI Prism 7300 Real-Time PCR System (Applied Biosystems). qPCR data were normalized to the level of TATA-box binding protein (TBP) messenger RNA (mRNA) and analyzed with LinRegPCR (v2017.1) to derive mean efficiency (N0) (Ruijter et al., 2009; Tuomi et al., 2010).

Transcriptome profiles were obtained for 6 liver samples per group at the GeT-TRiX facility (GénoToul, G  nopole Toulouse Midi-Pyr  n  es) using Sureprint G3 Mouse GE v2 microarrays (8  $\times$  60K, design 074809, Agilent Technologies), according to the manufacturer's instructions. For each sample, Cyanine-3 (Cy3) labeled cRNA was prepared from 200 ng of total RNA using the One-Color Quick Amp Labeling kit (Agilent Technologies), according to the manufacturer's instructions, followed by Agencourt RNAClean XP (Agencourt Bioscience Corporation, Beverly, Massachusetts). Dye incorporation and cRNA yield were determined using a Drop-sense 96 UV/VIS droplet reader (Trinean, Belgium). Next, 600 ng of Cy3-labeled cRNA were hybridized on the microarray slides, following the manufacturer's instructions. Immediately after washing, slides were scanned on an Agilent G2505C Microarray Scanner using Agilent Scan Control A.8.5.1 software and the fluorescence signal was extracted using Agilent Feature Extraction software v10.10.1.1 with default parameters. Microarray data and experimental details are available in NCBI's Gene Expression Omnibus (GEO) database (accession numbers GSE165699 and GSE165558).

### Histology

Paraformaldehyde-fixed, paraffin-embedded BAT was sliced into 3- $\mu$ m sections and stained with hematoxylin and eosin (H&E).

### UCP1 protein expression

Ten milligrams of BAT was homogenized in RIPA buffer (50 mM Tris-HCl, pH 7.4, 150 mM NaCl, 2 mM EDTA, 0.1% SDS, 1 mM PMSF, 1% NP40, 0.25% sodium deoxycholate, proteinase and phosphatase inhibitors) and centrifuged 30 min at 13,000 g. The protein concentration in supernatants was measured using a Pierce BCA Protein Assay Kit (Thermo Scientific). Proteins were denatured in Laemmli buffer (62.5 mM Tris HCl, pH 6.8, 2% SDS, 10% glycerol, 5%  $\beta$ -mercaptoethanol, 0.02% bromophenol blue), separated by SDS-polyacrylamide gel electrophoresis (12%), and transferred onto nitrocellulose membrane. The membrane was blocked with 5% BSA in TBST (10 mM Tris-HCl, 150 mM NaCl, 0.05% Tween 20). Immunodetection was performed using anti-UCP1 (1:1,000, Abcam, ab10983) and anti-Hsp90 (1:1,000, Cell Signaling, #4877) overnight at 4°C, followed by horseradish peroxidase-conjugated secondary antibody (anti-rabbit 1:5,000) for 1 h at room temperature. Signals were acquired using enhanced chemiluminescence using Clarity Western ECL Substrate (Bio-Rad) and a ChemiDoc Touch Imaging System (Bio-Rad).

### QUANTIFICATION AND STATISTICAL ANALYSES

Statistical analyses on biochemical and qPCR data were performed using GraphPad Prism for Windows (version 7.00; GraphPad Software). Two-way ANOVA was performed, followed by appropriate post-hoc tests (Sidak's multiple comparisons test) when differences were found to be significant ( $p < 0.05$ ). When only 2 groups were compared, the Student's t-test was used;  $p < 0.05$  was considered significant. \* or # $p < 0.05$ , \*\* or ## $p < 0.01$ , \*\*\* or ### $p < 0.001$ .

Microarray data were analyzed using R and Bioconductor packages (Huber et al., 2015) as described in GEO accession numbers GSE165699 and GSE165558. Raw data (median signal intensity) were filtered, log2 transformed, corrected for batch effects (microarray washing bath and labeling serials), and normalized using the qsmooth method (Hicks et al., 2018). A model was fitted using the limma lmFit function (Ritchie et al., 2015). Pair-wise comparisons between biological conditions were applied using specific



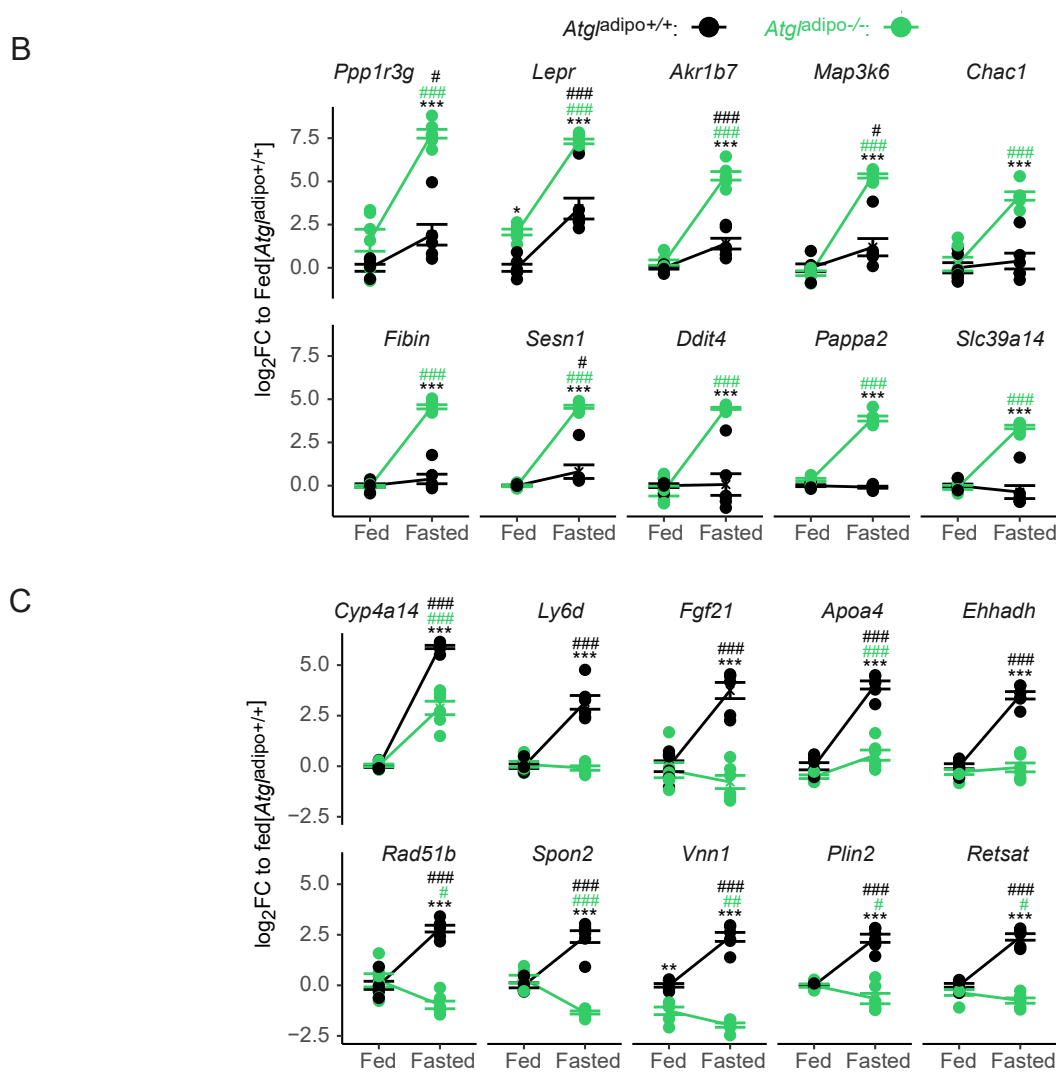
contrasts. A correction for multiple testing was applied using the Benjamini-Hochberg procedure ([Benjamini and Hochberg, 1995](#)) to control the false discovery rate (FDR). Probes with an  $FDR \leq 0.05$  were considered to be differentially expressed between conditions. Hierarchical clustering was applied to the samples and the differentially expressed probes using 1-Pearson correlation coefficient as distance and Ward's criterion for agglomeration. The clustering results are illustrated as a heatmap of expression signals. Gene ontology and transcription factor enrichment analysis were performed using Metascape ([Zhou et al., 2019](#)). Gene network analysis was performed using String (version 11.0) ([Szkarczyk et al., 2019](#)).

## Supplemental information

### ATGL-dependent white adipose tissue lipolysis

#### controls hepatocyte PPAR $\alpha$ activity

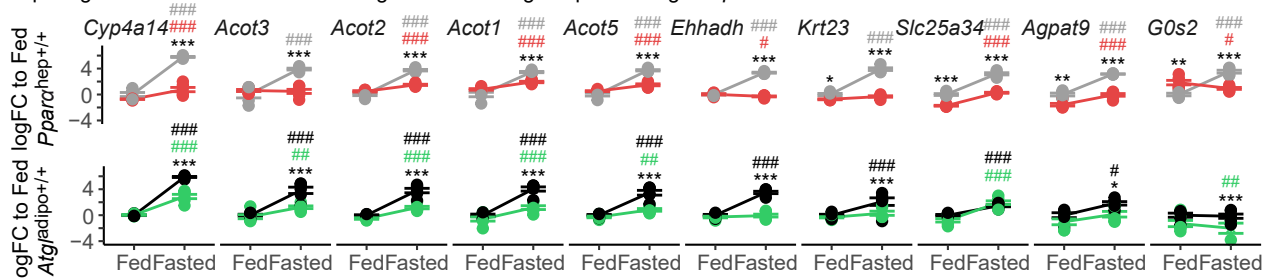
Anne Fougerat, Gabriele Schoiswohl, Arnaud Polizzi, Marion Régnier, Carina Wagner, Sarra Smati, Tiffany Fougeray, Yannick Lippi, Frederic Lasserre, Ilyès Raho, Valentine Melin, Blandine Tramunt, Raphaël Métivier, Caroline Sommer, Fadila Benhamed, Chantal Alkhoury, Franziska Greulich, Céline Jouffe, Anthony Emile, Michael Schupp, Pierre Gourdy, Patricia Dubot, Thierry Levade, Delphine Meynard, Sandrine Ellero-Simatos, Laurence Gamet-Payrastre, Ganna Panasyuk, Henriette Uhlénhaut, Ez-Zoubir Amri, Céline Cruciani-Guglielmacci, Catherine Postic, Walter Wahli, Nicolas Loiseau, Alexandra Montagner, Dominique Langin, Achim Lass, and Hervé Guillou



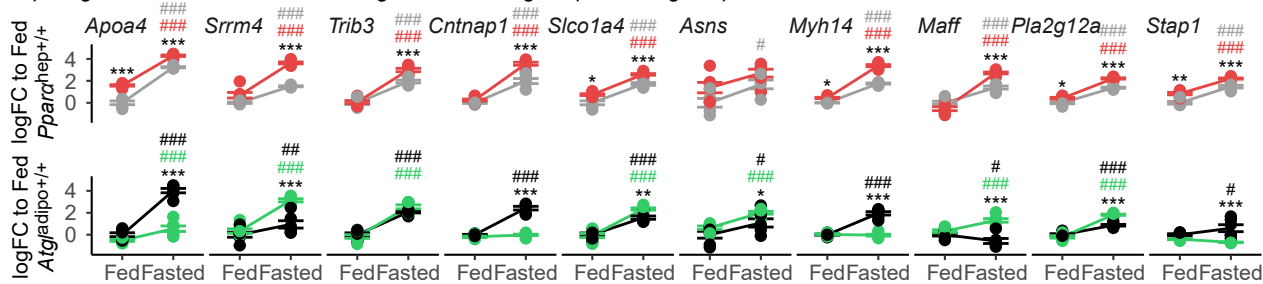
**Supplementary Figure S1: Adipocyte *Atgl* deficiency altered the fasting-induced hepatic gene expression.** Related to Figure 1. (A-D) Microarray experiment performed with liver samples from *Atgl*<sup>adipo+/+</sup> and *Atgl*<sup>adipo-/-</sup> mice fed *ad libitum* or fasted for 24 h (n = 6/group). (A) Principle component analysis (PCA) score plots of the whole transcriptomic dataset. (B) The 10 genes with the highest fold-change upon fasting in *Atgl*<sup>adipo-/-</sup> mice. (C) The 10 genes with the highest fold-changes upon fasting in *Atgl*<sup>adipo+/+</sup> mice. (D) Volcano plot representing differences in gene expression between *Atgl*<sup>adipo+/+</sup> and *Atgl*<sup>adipo-/-</sup> in response to fasting of selected target genes of PPARα. # fasting effect (colored by genotype), \* genotype effect, \* or # *adj. p* < 0.05, \*\* or ## *adj. p* < 0.01, \*\*\* or ### *adj. p* < 0.001.

*Ppar*<sup>hep+/+</sup>: *Ppar*<sup>hep-/-</sup>: *Atgl*<sup>adipo+/+</sup>: *Atgl*<sup>adipo-/-</sup>:

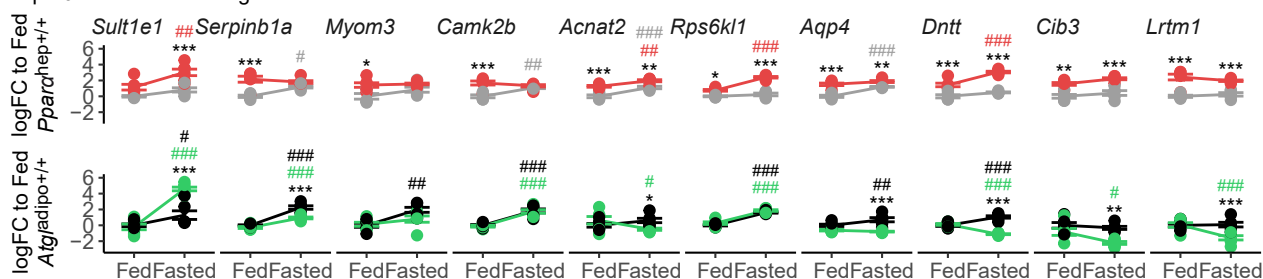
Top 10 genes from cluster 3 with the highest fold-changes upon fasting in *Ppar*<sup>hep+/+</sup> mice.



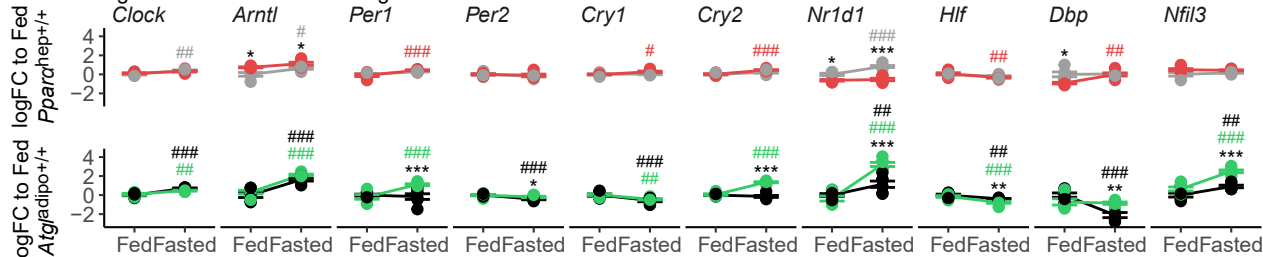
Top 10 genes from cluster 5 with the highest fold-changes upon fasting in *Ppar*<sup>hep-/-</sup> mice.



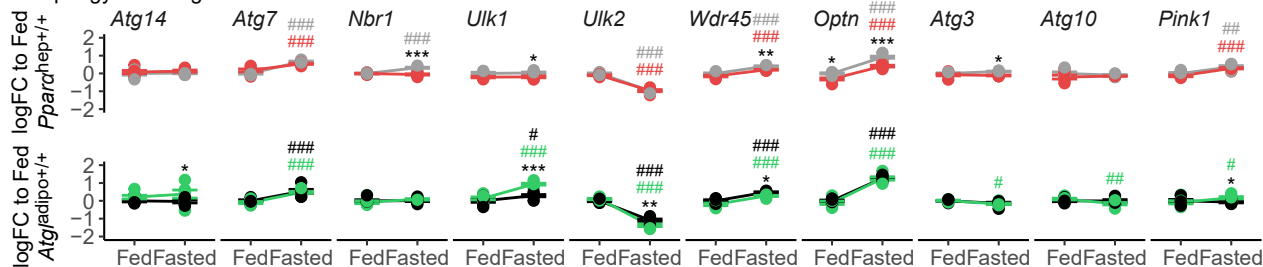
Top 10 most contrasted genes from cluster 4.



Core clock genes and clock-controlled genes.

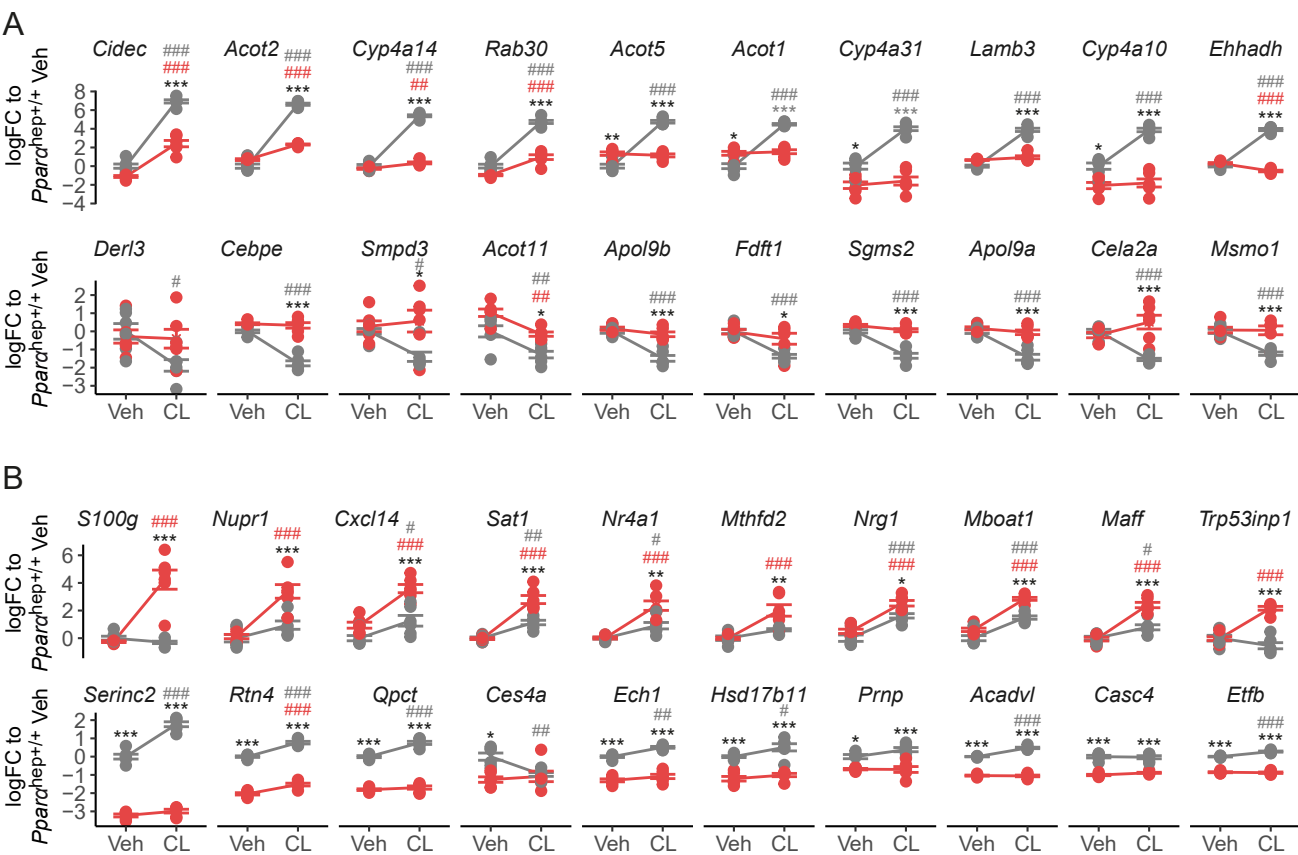


Autophagy-related genes.



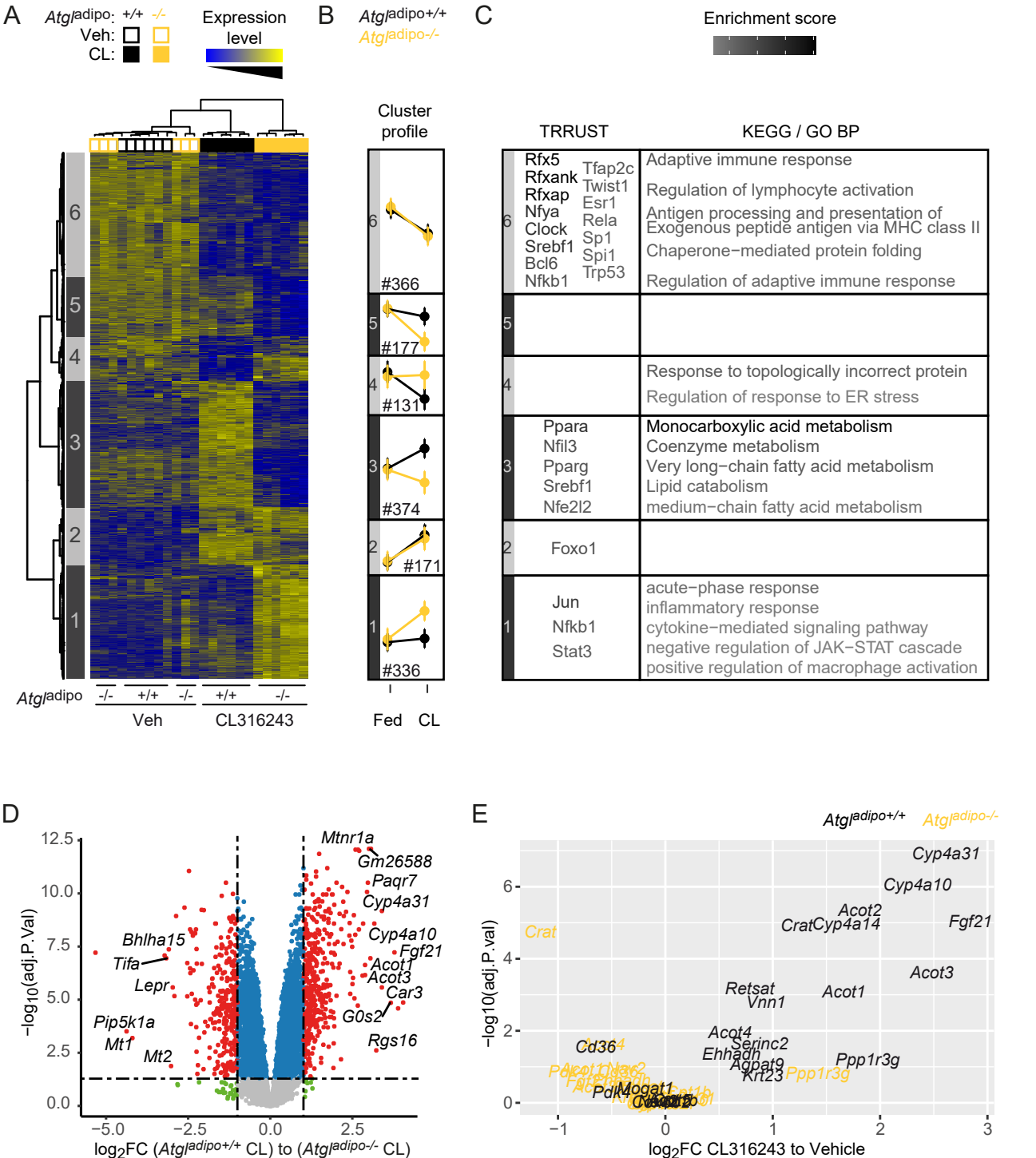
**Supplementary Figure S2: Fasting-induced PPARG-dependent hepatic gene expression analyzed in the *Atgl* deficient model.** Related to Figure 2. Microarray experiments performed with liver samples from *Atgl*<sup>adipo+/+</sup> and *Atgl*<sup>adipo-/-</sup> mice fed *ad libitum* or fasted for 24 h, and from *Ppar*<sup>hep+/+</sup> and *Ppar*<sup>hep-/-</sup> mice fed *ad libitum* or fasted for 24 h (n = 6/group). # fasting effect (colored by genotype), \* genotype effect, \* or # *adj.p* < 0.05, \*\* or ## *adj.p* < 0.01, \*\*\* or ### *adj.p* < 0.001.

*Ppara*<sup>hep+/+</sup>: ● *Ppara*<sup>hep-/-</sup>: ●

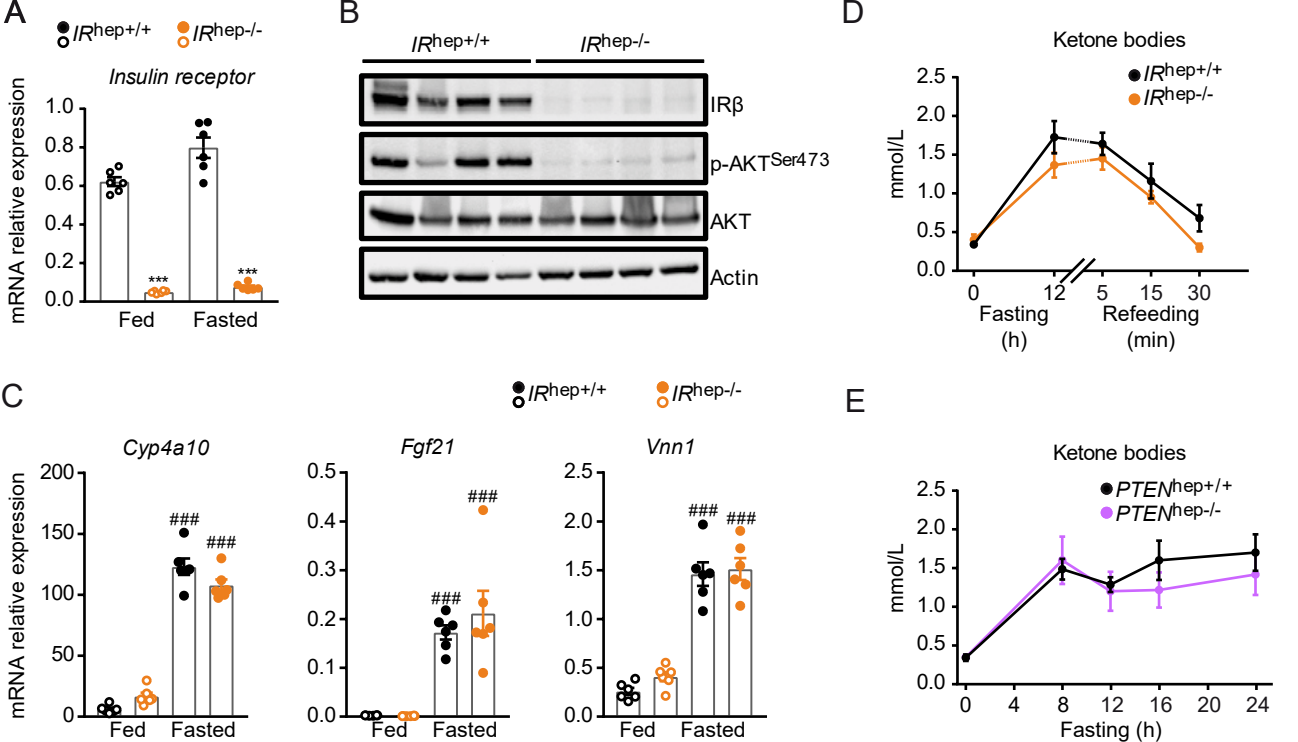


**Supplementary Figure S3: Hepatocyte *Ppara* deficiency altered hepatic gene expression in response to  $\beta_3$ -adrenergic receptor stimulation.** Related to Figure 3. **(A-B)** Microarray experiment performed with liver samples from *Ppara*<sup>hep+/+</sup> and *Ppara*<sup>hep-/-</sup> fed mice treated with CL316243 (3 mg/kg body weight) or vehicle by gavage for 6 hours (n=6/group). **(A)** Fold-changes of the 10 genes most upregulated (cluster 2) and of the 10 genes most downregulated by CL316243 (cluster 5) in *Ppara*<sup>hep+/+</sup> mice. **(B)** Fold-changes of the 10 genes most upregulated (cluster 6) and of the 10 genes most downregulated (cluster 3) by CL316243 in *Ppara*<sup>hep-/-</sup> mice. # CL316243 effect (colored by genotype), \* genotype effect, \* or # *adj.p* < 0.05, \*\* or ## *adj.p* < 0.01, \*\*\* or ### *adj.p* < 0.001.



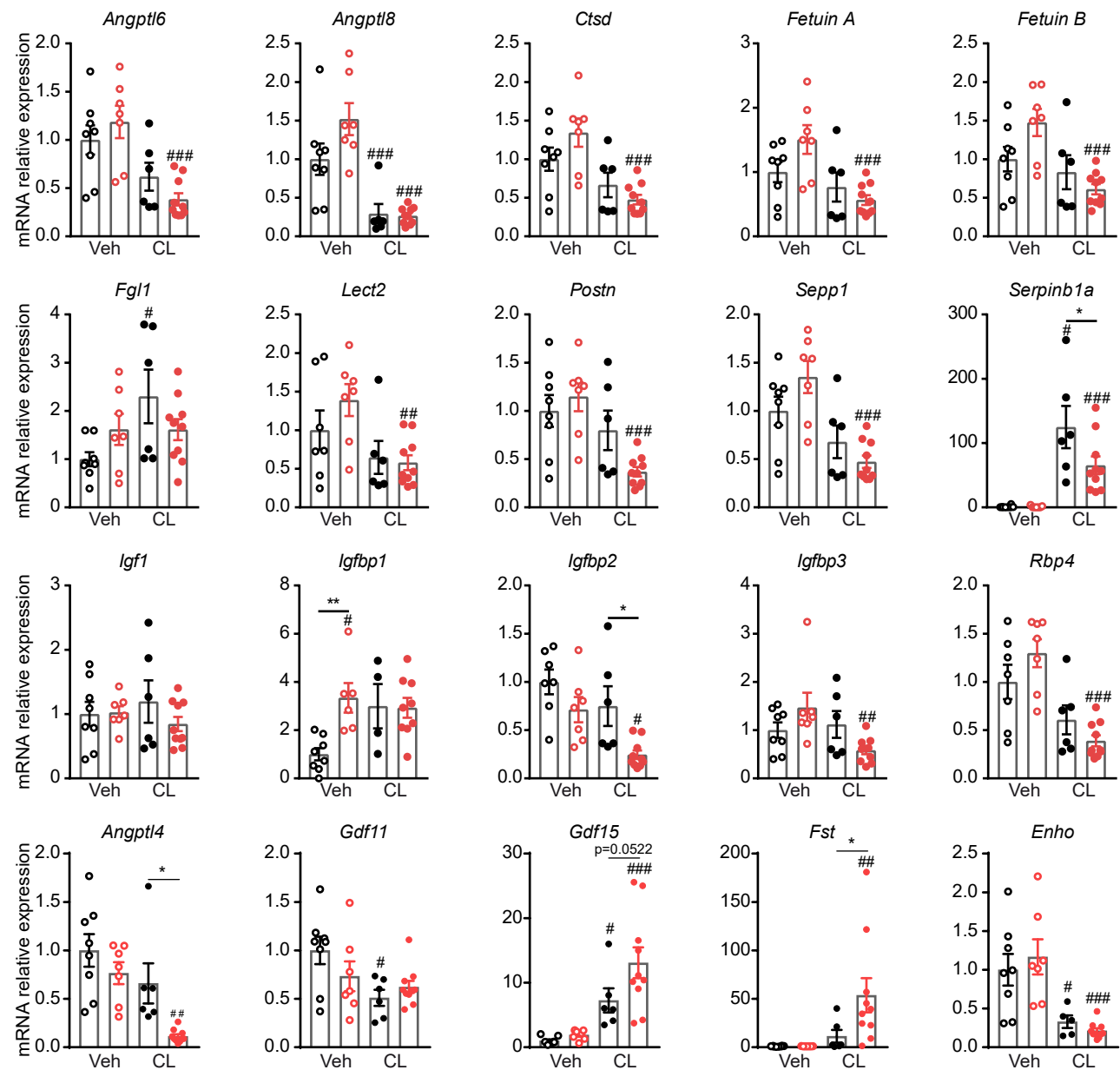


**Supplementary Figure S4: Adipocyte *Atgl* deficiency altered hepatic gene expression in response to  $\beta$ 3-adrenergic receptor stimulation.** Related to Figure 3. **(A-E)** Microarray experiment performed with liver samples from *Atgl*<sup>adipo</sup>+/+ and *Atgl*<sup>adipo</sup>-/- fed mice treated with CL316243 (3 mg/kg body weight) or vehicle by gavage for 6 hours (n = 6/group). **(A)** Heatmap with hierarchical clustering shows the definition of 6 gene clusters (FC > 2;  $p \leq 0.05$ ). **(B)** Schematic representation of the mean cluster profiles in each cluster (unique Entrez gene ID from Metascape). **(C)** Gene Ontology (GO) analysis and enrichment of transcription factors (TF) of genes in each heatmap clusters (FC > 2;  $adj.p < 0.05$ ). **(D)** Volcano plot of differences in gene expression between *Atgl*<sup>adipo</sup>+/+ and *Atgl*<sup>adipo</sup>-/- in response to CL316243 treatment. **(E)** Volcano plot representing differences in gene expression between *Atgl*<sup>adipo</sup>+/+ and *Atgl*<sup>adipo</sup>-/- in response to CL316243 treatment of selected target genes of PPAR $\alpha$ .

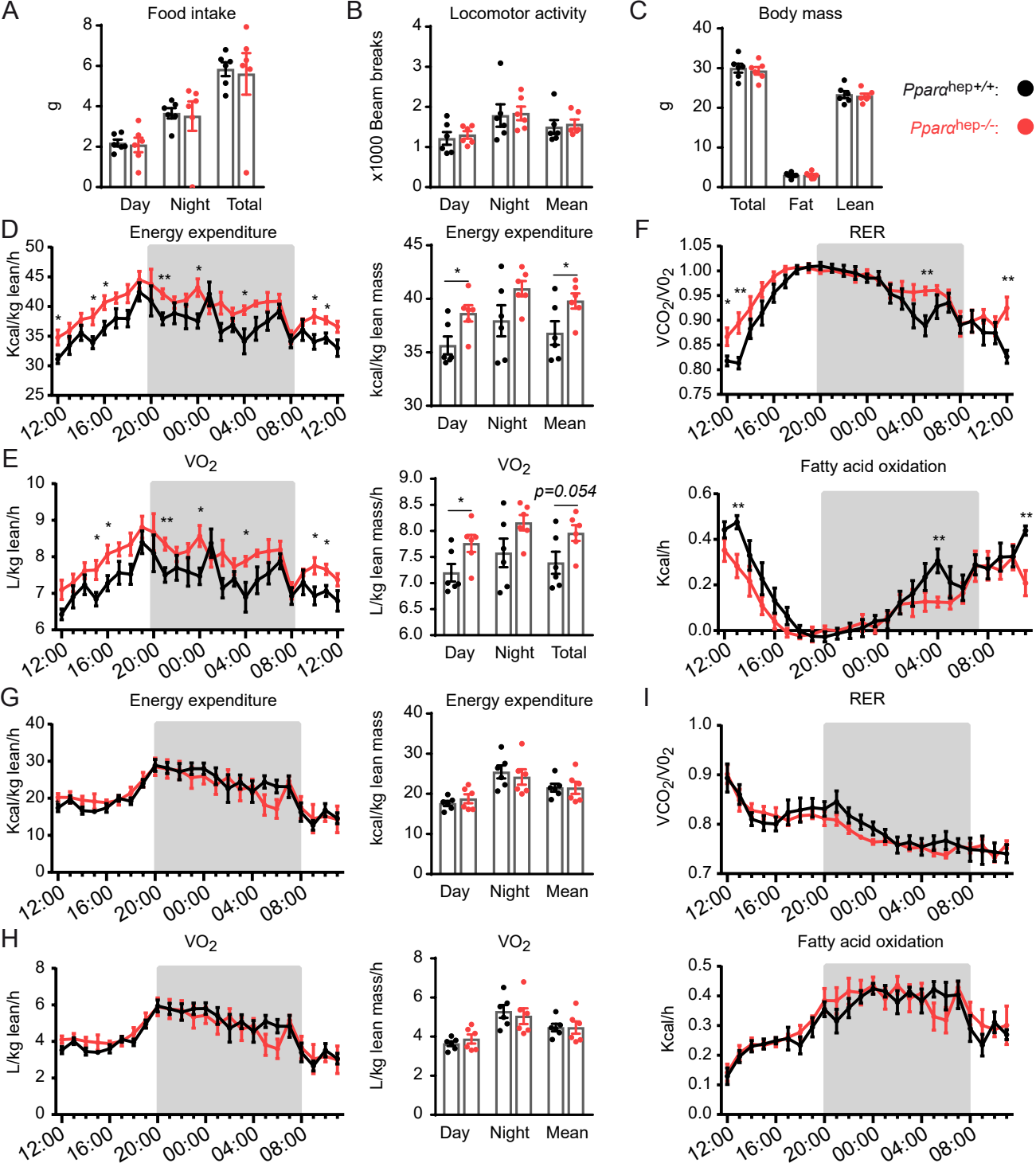


**Supplementary Figure S5: Modulation of hepatocyte insulin signaling does not influence hepatocyte PPAR $\alpha$ -dependent responses in the liver during fasting and refeeding.** Related to STAR Methods. **(A)** mRNA relative expression of Insulin receptor measured by qRT-PCR in the liver of  $IR^{hep+/+}$  and  $IR^{hep-/-}$  mice fed *ad libitum* or fasted for 24 h. **(B)** Western blot analysis of Insulin receptor  $\beta$  (IR $\beta$ ), phosphorylated AKT, total AKT and  $\beta$ -actin in the liver of  $IR^{hep+/+}$  and  $IR^{hep-/-}$  mice fed *ad libitum*. **(C)** mRNA relative expression of *Cyp4a10*, *Vnn1* and *Fgf21* measured by qRT-PCR in the liver of  $IR^{hep+/+}$  and  $IR^{hep-/-}$  mice fed *ad libitum* or fasted for 24 h. **(D)** Circulating levels of ketone bodies ( $\beta$ -hydroxybutyrate) of  $IR^{hep+/+}$  and  $IR^{hep-/-}$  in the fed and fasted state, and after 5, 15 and 30 min of refeeding. **(E)** Circulating levels of ketone bodies ( $\beta$ -hydroxybutyrate) in  $PTEN^{hep+/+}$  and  $PTEN^{hep-/-}$  fasted for 0, 8, 12, 16 and 24 h. Results are the mean  $\pm$  SEM. # fasting effect, \* genotype effect. \* or #  $p < 0.05$ , \*\* or ##  $p < 0.01$ , \*\*\* or ###  $p < 0.001$ .

*Ppara*<sup>hep+/+</sup>: Veh ○ CL ● *Ppara*<sup>hep-/-</sup>: Veh ○ CL ●



**Supplementary Figure S6: Relative gene expression of *Angptl6*, *Angptl8*, *Ctsd*, *Fetuin A*, *Fetuin B*, *Fgl1*, *Lect2*, *Postn*, *Sepp1*, *Serpinb1a*, *Igf1*, *Igfbp1*, *Igfbp2*, *Igfbp3*, *Rbp4*, *Angptl4*, *Gdf11*, *Gdf15*, *Fst* and *Enho*.** Related to Figure 4. Gene expression was measured by qRT-PCR in fasted *Ppara*<sup>hep+/+</sup> and *Ppara*<sup>hep-/-</sup> mice treated with CL316243 (3 mg/kg body weight) or vehicle by gavage for 6 hours. Data are means  $\pm$  SEM. # CL316243 effect, \* genotype effect, \* or #  $p < 0.05$ , \*\* or ##  $p < 0.01$ , \*\*\* or ###  $p < 0.001$ .



**Supplementary figure S7: Calorimetry for *Ppara*<sup>hep+/+</sup> and *Ppara*<sup>hep-/-</sup> mice during 24 h of cold exposure at 7°C or 24 h of fasting.**

(Related to Figure 4. (A–F) *Ppara*<sup>hep+/+</sup> and *Ppara*<sup>hep-/-</sup> mice were individually housed in a calorimetric cage and exposed to 7°C for 24 h. (A) Cumulative food intake calculated in total and during the light and dark phase. (B) Locomotor activity calculated in mean and during the light and dark phase. (C) Body composition. (D) Energy expenditure normalized per lean body mass. Bar graph (right panel) represents the average of energy expenditure during the light and dark phase in each group. (E) Rate of  $VO_2$  consumption normalized per lean body mass. Bar graph (right panel) represents the average of  $O_2$  consumption during the light and dark phase in each group. (F) Respiratory exchange ratio (RER) and fatty acid oxidation rate. (G–L) *Ppara*<sup>hep+/+</sup> and *Ppara*<sup>hep-/-</sup> mice were individually housed in a calorimetric cage and fasted for 24 h. (G) Energy expenditure normalized per lean body mass. Bar graph (right panel) represents the average of energy expenditure during the light and dark phase in each group. (H) Rate of  $VO_2$  consumption normalized per lean body mass. Bar graph (right panel) represents the average of  $O_2$  consumption during the light and dark phase in each group. (I) Respiratory exchange ratio (RER) and fatty acid oxidation rate. Results are the mean  $\pm$  SEM. \* genotype effect, \*  $p < 0.05$ , \*\*  $p < 0.01$ .

**Supplementary Table S1. Oligonucleotide sequences for real-time qPCR.  
Related to STAR methods**

Gene	NCBI Refseq	Forward primer	Reverse primer
<i>Angptl4</i>	NM_020581.2	TTCCCTGCCCTTCTCTACTTG	TACAGGTACCAAACCACCAGCC
<i>Angptl6</i>	NM_145154.2	GAATTGCCGCAAACCTCACT	ATGGCCGTCACCTCTCACAG
<i>Angptl8</i>	NM_001080940.1	CCCACCAAGAATTTGAGACCTT	ACTGTTGCTGCTCTGCCATCT
<i>Ctsd</i>	NM_009983	CTTCGTCTCCTTCGCGATTAT	GTCCGACGGATAGATGTGAACTT
<i>Cyp4a10</i>	NM_010011	TCCAGCAGTTCCCATCACCT	TTGCTTCCCAGAACCATCT
<i>Cyp4a14</i>	NM_007822	TCAGTCTATTTCTGGTGTGTTT	GAGCTCCTTGCTCTCAGATGGT
<i>Dio2</i>	NM_010050.4	ACAGCTTCCTCCTAGATGCCTACA	GGGAGCATCTTCACCCAGTTT
<i>Ehhadh</i>	NM_023737	CGTCTCCTCGGTTGGTGTTT	ATTATCTTCTTTGCAGTATCTAGCTGCTT
<i>Elovl3</i>	NM_007703	GCCTCTCATCCTCTGGTCCT	TGCCATAAACTTCACATCCT
<i>Enho</i>	NM_027147	CCGGGCTCAACTCAGGC	TGGTGCTCCTGTCCACACAC
<i>FetuinA</i>	NM_013465	ATCGACAAAGTCAAGGTGTGGTCT	TGTCAACTTCCATCTCATACACCACT
<i>FetuinB</i>	NM_021564	CTCGTCAAAGTCACCAAGGCTAT	CACATAGTAAGCAGGGCCAGAC
<i>Fgl1</i>	NM_145594.2	TGCAAACCTGAACGGTGTGTTT	TTCAAGGAATACCACCACCCA
<i>Fgf21</i>	NM_020013.4	AAAGCCTCTAGGTTTCTTTGCCA	CCTCAGGATCAAAGTGAGGCG
<i>Fst</i>	NM_008046.2	TGCTGCTACTCTGCCAGTTCAT	CACCTCTCCTTGCTCAGTCTGTCT
<i>Gadd45a</i>	NM_007836	GCGCAGACCCCGGAC	TCCATGTAGCGACTTTCCCG
<i>Gdf15</i>	NM_011819	GCTGTCCGGATACTCAGTCCA	TTGACGCGGAGTAGCAGCT
<i>Igf1</i>	NM_0105124	GATCTGCCTCTGTGACTTCTTGAA	CAGGTAGAAGAGGTGTGAAGACGA
<i>Igfbp1</i>	NM_008341.4	CCTGCCAACGAGAACTCTAT	AGGGATTTTCTTTCCACTCC
<i>Igfbp2</i>	NM_008342	GCATGGCCGGTACAACCTTA	GCTGTCCGTTTACAGAGACATCTT
<i>Igfbp3</i>	NM_008343	CAGGCAGCCTAAGCACCTAC	CTCCTCGGACTCACTGATGTTTC
<i>Inhbe</i>	NM_008382.3	TCAGCTTTGCTACCATCATAGACA	CATGGAGCGGTAGGTTGAAGT
<i>Lect2</i>	NM_010702	GTGGACAGTACTCTGCTCAAA	TCCCAGTGAATGGTGCATAC
<i>Pgc1α</i>	NM_008904	CAATCGGAAATCATATCCAACCA	CTGTGAGGACCGTAGGAAGT
<i>Pparα</i>	NM_011144	CCCTGTTTGTGGCTGCTATAATTT	GGGAAGAGGAAGGTGTCATCTG
<i>Pparα (genotyping)</i>	NM_011144	GTACCACTACGGAGTTC	GAATAGTTCGCCGAAAG
<i>Postn</i>	NM_015784	GAATGCTGCCCTGGCTATATGA	AATGCCAGCGTGCCATAAA
<i>Prdm16</i>	NM_027504.3	TCCGCGGTACGCAATAGC	TCACTGCCATCCGACATGTC
<i>Rbp4</i>	NM_011255	GCCAAGTTCAAGATGAAGTACTGG	TGTCGTAGTCCGTGTCGATGA
<i>Sepp1</i>	NM_009155	AAGATCGCTTACTGTGAGGAGAGG	GCTGAGGTCACAGTTTTACAGAAGTC
<i>Serpina1a</i>	NM_025429	GGACGAGTCCACGGGTCTTA	AGTTTGACGTGGACATCAATGAATTC
<i>Tbp</i>	NM_013684	ACTTCGTGCAAGAAATGCTGAA	GCAGTTGTCCGTGGCTCTCT
<i>Ucp1</i>	NM_009463.3	CCTGCCTCTCTCGGAAACAA	TGTAGGCTGCCCAATGAACA